ESC European Society of Cardiology

Cardiovascular Research (2024) **120**, 927–942
https://doi.org/10.1093/cvr/cvae054

Proteomics couples electrical remodelling to inflammation in a murine model of heart failure with sinus node dysfunction

Konstantin Kahnert [1†], Luca Soattin[2†], Robert W. Mills[1†], Claire Wilson[2,3†], Svetlana Maurya[1], Andrea Sorrentino[1], Sami Al-Othman[2], Roman Tikhomirov[2,4], Yordi J. van de Vegte[5], Finn B. Hansen[1], Jonathan Achter[1], Wei Hu[6], Min Zi[2], Matthew Smith[2,4], Pim van der Harst [5,7,8,9], Morten S. Olesen[1], Kristine Boisen Olsen[10], Jytte Banner [10], Thomas H.L. Jensen[11], Henggui Zhang[6], Mark R. Boyett[12‡], Alicia D'Souza[2,4]*‡, and Alicia Lundby [1]*‡

[1]Department of Biomedical Sciences, Faculty of Health and Medical Sciences, University of Copenhagen, Blegdamsvej 3B, 2200, Copenhagen N, Denmark; [2]Division of Cardiovascular Sciences, University of Manchester, Core Technology Facility, 46 Grafton Street, Manchester, M13 9NT, UK; [3]Institute of Systems, Molecular & Integrative Biology, University of Liverpool, Liverpool, UK; [4]National Heart and Lung Institute, Imperial College London, Imperial Centre for Translational and Experimental Medicine (ICTEM), 72 Du Cane Road, London W12 0NN, UK; [5]Department of Cardiology, University of Groningen, University Medical Center Groningen, Groningen, the Netherlands; [6]Department of Physics & Astronomy, Biological Physics Group, University of Manchester, Manchester, UK; [7]Department of Cardiology, University Medical Center Utrecht, Utrecht, the Netherlands; [8]Department of Genetics, University of Groningen, University Medical Center Groningen, Groningen, the Netherlands; [9]Durrer Center for Cardiogenetic Research, Netherlands Heart Institute, Utrecht, the Netherlands; [10]Department of Forensic Medicine, University of Copenhagen, Rigshospitalet, Copenhagen, Denmark; [11]The Heart Center, Rigshospitalet, Copenhagen, Denmark; and [12]Faculty of Life Sciences, University of Bradford, Bradford, UK

Received 1 November 2023; revised 22 December 2023; accepted 8 January 2024; online publish-ahead-of-print 25 April 2024

Time of primary review: 20 days

Aims In patients with heart failure (HF), concomitant sinus node dysfunction (SND) is an important predictor of mortality, yet its molecular underpinnings are poorly understood. Using proteomics, this study aimed to dissect the protein and phosphorylation remodelling within the sinus node in an animal model of HF with concurrent SND.

Methods and results We acquired deep sinus node proteomes and phosphoproteomes in mice with heart failure and SND and report extensive remodelling. Intersecting the measured (phospho)proteome changes with human genomics pharmacovigilance data, highlighted downregulated proteins involved in electrical activity such as the pacemaker ion channel, Hcn4. We confirmed the importance of ion channel downregulation for sinus node physiology using computer modelling. Guided by the proteomics data, we hypothesized that an inflammatory response may drive the electrophysiological remodeling underlying SND in heart failure. In support of this, experimentally induced inflammation downregulated Hcn4 and slowed pacemaking in the isolated sinus node. From the proteomics data we identified proinflammatory cytokine-like protein galectin-3 as a potential target to mitigate the effect. Indeed, *in vivo* suppression of galectin-3 in the animal model of heart failure prevented SND.

Conclusion Collectively, we outline the protein and phosphorylation remodeling of SND in heart failure, we highlight a role for inflammation in electrophysiological remodelling of the sinus node, and we present galectin-3 signalling as a target to ameliorate SND in heart failure.

* Corresponding authors. Tel: +44(0) 207 594 8616, E-mail: alicia.dsouza@manchester.ac.uk (A.D.); Tel: +45 35 32 7900, E-mail: alicia.lundby@sund.ku.dk (A.L.)
† These authors contributed equally to this work.
‡ These authors contributed equally to this work.

Graphical Abstract

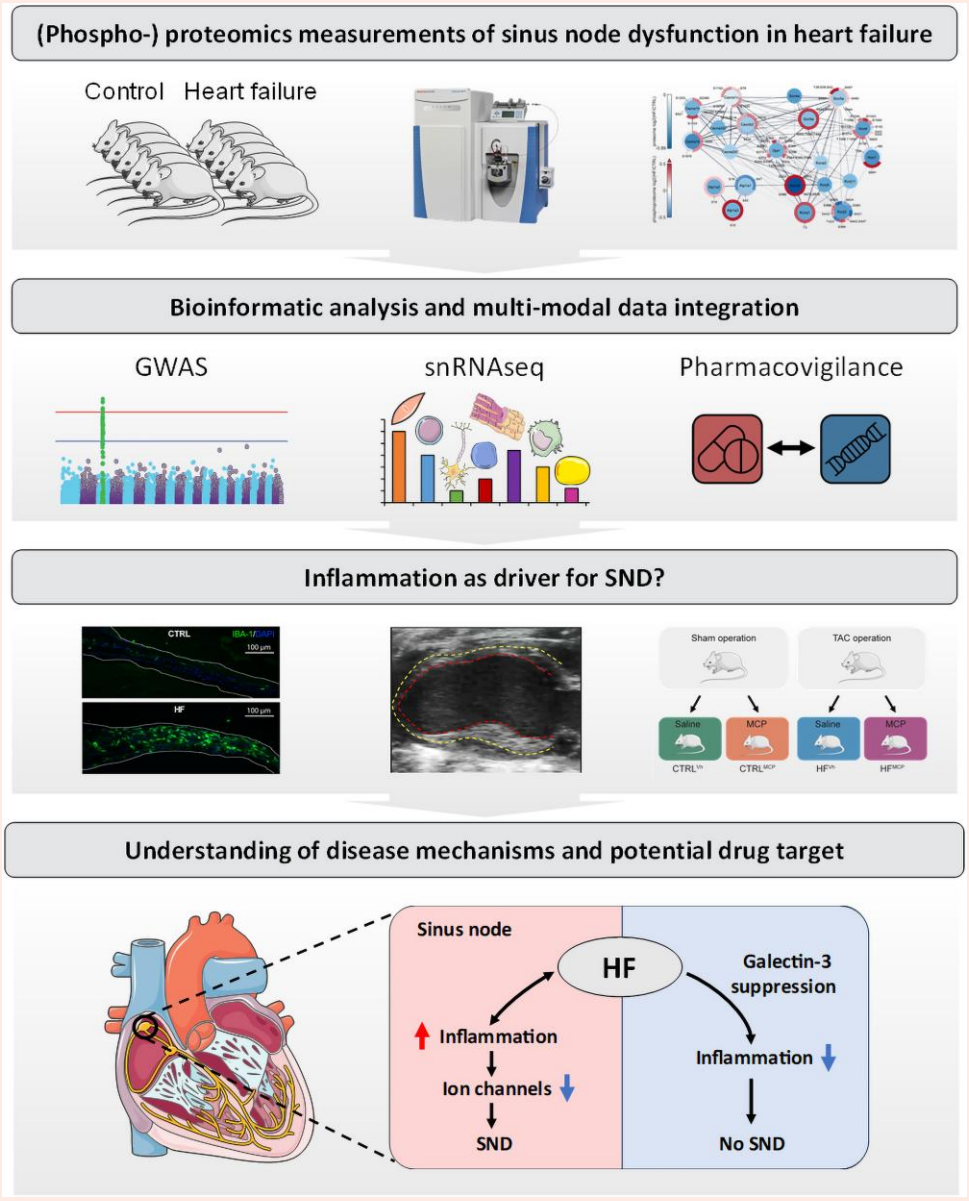

Keywords Proteomics • Sinus node dysfunction • Heart failure • Inflammation • Galectin-3 • Multi-omics data integration

1. Introduction

Heart failure (HF) is a global health problem and one of the leading causes of hospitalization in USA and Europe, resulting in over 1 million admissions/year as a primary diagnosis.[1,2] Despite advances in therapy, sudden death is the principal cause of mortality in ambulatory HF patients with reduced ejection fraction.[3] While most commonly attributed to ventricular arrhythmias, bradyarrhythmias are an important yet underappreciated cause, given to account for up to 10–30% of cardiac sudden deaths in the hospital.[4–8] In these studies, electrocardiogram (ECG) monitoring during episodes of sudden death showed that cardiac arrests were characterized not by tachyarrhythmia but by a terminal bradyarrhythmia. The development of atrioventricular block or sinus bradycardia was the strongest predictor of mortality.[8]

HF in humans and animal models results in sinus node dysfunction (SND) characterised by a decrease in intrinsic heart rate, increase in sino-atrial conduction time, increased incidence of sinus node exit block, increase in corrected sinus node recovery time (cSNRT), caudal shift of the leading pacemaker site, and fractionation of electrograms.[9–16] SND can also lead to chronotropic incompetence, which is common in HF.[17–19] As bradycardia alone can result in HF,[20–24] it is likely that SND in HF exacerbates the underlying pathology.

SND in HF is understood to be the result of transcriptional remodelling of ion channels, resulting in a reduction of the corresponding ionic currents,[10,11,25,26] alongside apoptosis and fibrosis.[27–29] However there has been no systematic study of the protein and signalling changes that accompany SND in HF, and importantly, no exploration of the drivers of the remodelling changes.

To address this knowledge gap, we applied a data-driven approach to outline the global protein- and signalling changes of the sinus node in the well-characterised mouse transverse aortic constriction (TAC) model of HF. We report substantial remodelling of the sinus node proteome in HF, characterised by a widespread down-regulation of ion channels critical to electrical activity and a major inflammatory response with considerable macrophage expansion. We assessed experimentally whether inflammation and SND in HF are mechanistically linked and show that activation of inflammation in the isolated sinus node slows pacemaking. To test if inhibition of the inflammatory response could present a strategy to prevent SND in HF, we identified a potential target from the proteomics data: the pro-inflammatory beta-galactoside-binding lectin, galectin-3, expressed and secreted by macrophages.[30] We show that systemic inhibition of galectin-3 ameliorates SND in the animal model of HF. Our study reveals the protein remodelling that underlies SND in HF, provides proof-of-concept for inflammation as a driver and potential therapeutic target in SND, and suggests a pharmacological target of relevance to disease.

2. Methods

2.1 Animal experiments

8-week-old male C57BL/6N mice were used, and all animal studies were performed in accordance with the UK Scientific Procedures Act 1986 and Directive 2010/63/EU of the European Parliament. Ethical approval was provided by the University of Manchester Ethics Committee. To produce a model of pressure overload-induced heart failure, mice underwent transverse aortic constriction (HF group) or a sham operation (CTRL group).[31] Body weight and conscious heart rate measurements were collected every week following surgery. At 8 weeks post-surgery, mice underwent an echocardiography assessment and an unconscious ECG was performed prior to termination.

2.2 Proteome and phosphoproteome measurements

Sinus node (SN) samples were collected from 15 mice from the HF group as well as from the CTRL group. Sample preparation was carried out as described earlier.[32,33] Briefly, tissue samples were homogenized, proteins extracted and enzymatically digested into peptides, isobarically labelled using tandem mass tags (TMT) and pooled. Part of the combined sample was subjected to phosphopeptide enrichment, before enriched and remaining samples were each fractionated and measured by reversed-phase liquid chromatography tandem mass spectrometry (LC-MS/MS) to obtain proteome and phosphoproteome measurements.

2.3 Data analysis and multi-modal data integration

After careful quality control, proteomics data were log2-tranformed, normalised, and missing values were imputed before performing differential expression analyses, functional enrichment analyses of differential expressed/phosphorylated proteins/phosphosites as well as a kinase-substrate enrichment analysis. Two single-cell/single-nucleus RNA sequencing data sets,[32,34] were utilized to predict the cell type of origin of significantly differentially expressed proteins. To assess regulation of particular translational value, we cross-referenced our (phospho)proteomics data with complementary human datasets. We intersected our data with heart rate-associated genes identified through a genome-wide association study performed on data from the UK Biobank. Furthermore, we examined the interaction between these proteins and drugs associated with bradycardia. This was determined through analysis of reported adverse events associated with pharmaceutical use by consulting the FDA Adverse Event Reporting System (FAERS) and a drug-gene interaction database (DGIdb),[35] and employing a multivariable logistic regression model we previously developed.[36]

2.4 Functional evaluation of inflammation in SND

To confirm findings made, we performed immunolabelling and western blot experiments of mouse sinus node preparations from HF and CTRL animals, and recorded intracellular action potentials in isolated sinus nodes that were incubated with lipopolysaccharide (LPS) using sharp microelectrodes. Additionally, in two independent animal cohorts, HF and CTRL animals were randomised into vehicle and anti-galectin-3 treatment groups. Animals in the anti-galectin-3 group received modified citrus pectin (MCP) in the drinking water. Effect of treatment was evaluated by echocardiography as well as extracellular mapping of the electrical impulse in isolated sinus node preparations from both groups.

2.5 Statistical analysis of animal work

Statistical analysis was carried out using GraphPad Prism v9 (GraphPad Software, Inc.). If sample size was ≥8 (minimum sample size for a D'Agostino & Pearson test and Anderson–Darling test in GraphPad Prism), normal distribution of data was tested using D'Agostino & Pearson test, Anderson–Darling test, Shapiro–Wilk test, and Kolmogorov–Smirnov test. Equal variance was tested using the *F*-test. When both criteria were fulfilled, an unpaired Student's *t*-test (two-sided) was used to test for differences between sham- and TAC-operated mice. If the data were normally distributed but had unequal variance an unpaired *t*-test (two-sided) with Welch's correction was used and when the null hypothesis of normality was rejected or sample size was too low, the non-parametric Mann–Whitney *U* test was used. Differences between heart rate at different time points post-surgery were tested using a two-way analysis of variance (ANOVA), with a Bonferroni *post hoc* test. To test for differences between the four experimental groups in the modified citrus pectin (MCP) treatment experiment a two-way ANOVA with interaction effects and Tukey's multiple comparisons test with all six comparisons was used. In figures, data are shown as mean ± S.E.M. A *P*-value of <0.05 was regarded as significant, with asterisks indicating significance on figures (*$P < 0.05$; **$P < 0.01$; ***$P < 0.001$; ****$P < 0.0001$).

Methods and materials of the study are provided in full in the supplementary material.

3. Results

3.1 Deep proteome and phosphoproteome profiling of the sinus node in a mouse model of heart failure

To investigate protein and phosphorylation remodelling characterising SND in HF, we pursued quantitative proteome and phosphoproteome measurements of sinus nodes from mice of the C57BL/6N strain subjected to TAC or sham surgery. The C57BL/6N strain was used because it is more susceptible to heart failure than the more common C57BL/6J strain.[31] Eight weeks post-surgery, TAC-operated mice showed evidence of heart failure (decreased ejection fraction and fractional shortening, congestion of the lungs as shown by an increase in the lung weight to body weight ratio, dyspnoea, lethargy, and >20% weight loss), hypertrophy (increased heart weight to tibia length ratio, left ventricular mass and interventricular septum thickness in diastole) and electrical remodelling (decreased heart rate and increased PR interval, QRS duration, and QT and corrected QT intervals) (*Figure 1A*; Supplementary material online, *Figure S1*). Electrophysiological study of the isolated sinus node showed that the sinus node of TAC-operated mice was dysfunctional: the spontaneous beating rate was slowed, and the cSNRT was increased (*Figure 1B*). Additionally, activation mapping experiments revealed that, as in humans with HF, TAC-operated mice presented with a caudal shift of the leading pacemaker site, slower sinoatrial conduction, and increased prevalence of fractionated electrograms as discussed later (*Figure 5*). The two groups of mice are referred to as 'HF' for the TAC-operated animals and 'CTRL' for the sham-operated animals.

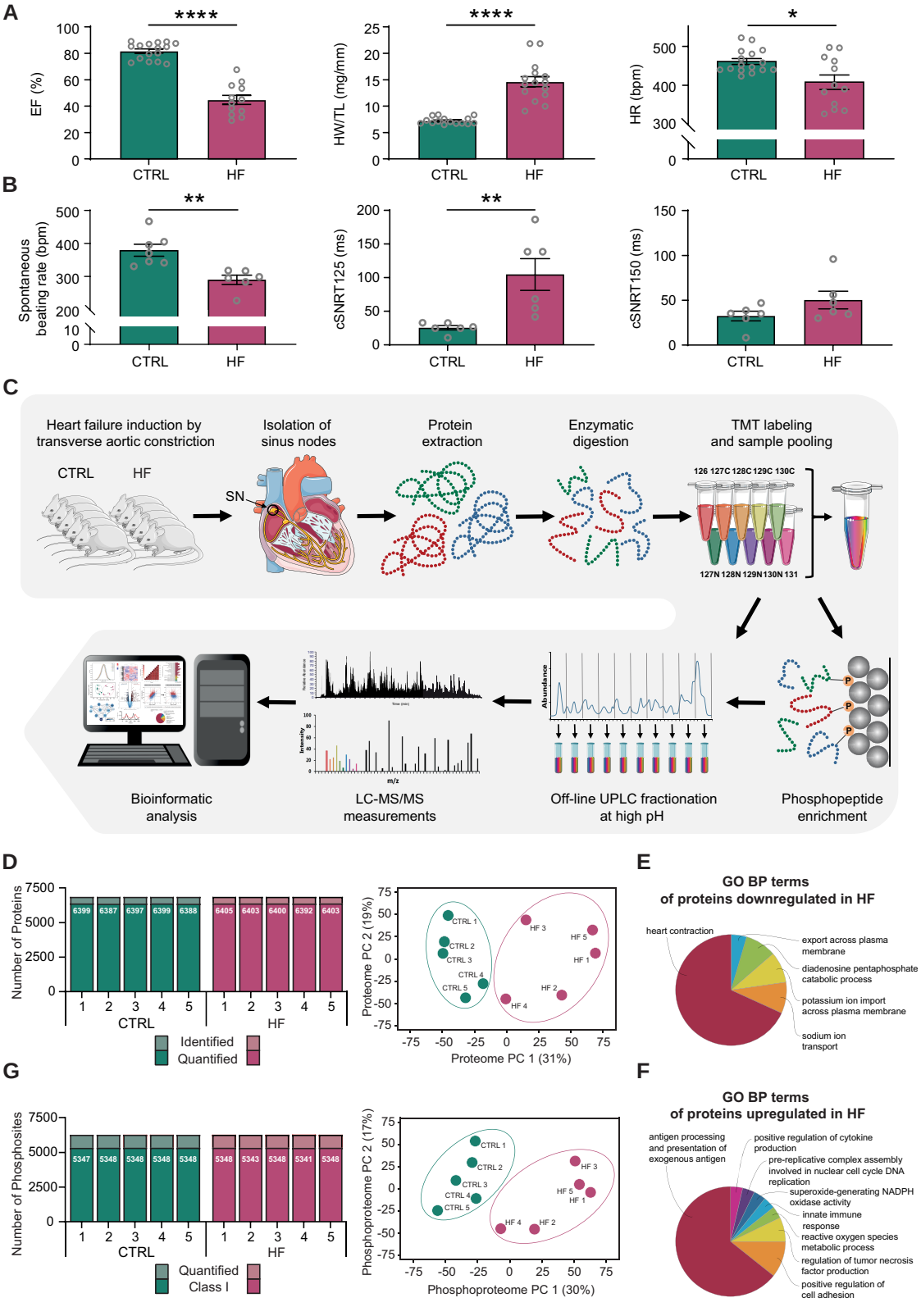

Figure 1 Physiological measurements, experimental workflow, and proteome and phosphoproteome measurements. (*A*) Physiological measurements from CTRL and HF mice. Left: ejection fraction (EF; ****$P < 0.0001$, Mann–Whitney *U* test); middle: heart weight/tibia length (HW/TL; ****$P < 0.0001$, Mann–Whitney *U* test); right: heart rate of anaesthetized animals (HR; *$P < 0.05$, Welch's *t*-test). Mean (±S.E.M.) shown as well as the individual data points ($n = 16/11, 15/15, 16/12$). (*B*) Electrophysiological measurements from the isolated sinus node of CTRL and HF mice. Left, spontaneous beating rate in beats/-min (bpm; **$P < 0.01$, Mann–Whitney *U* test). Middle, corrected sinus node recovery time after stimulation at a cycle length of 125 ms ($cSNRT_{125}$; (continued)

Figure 1 Continued

***$P < 0.001$, Mann–Whitney U test). Right, corrected sinus node recovery time after stimulation at a cycle length of 150 ms ($cSNRT_{150}$; not significant, Mann–Whitney U test). Mean (±S.E.M.) shown as well as the individual data points ($n = 7/6, 6/6, 6/6$). (*C*) Experimental workflow. HF was induced by TAC surgery and CTRL mice received a sham surgery. Eight weeks later, sinus nodes were isolated, proteins were extracted, digested, isobarically labelled using TMT and combined. Part of the combined sample was subjected to phosphopeptide enrichment prior to fractionation (for phosphoproteome measurement), part was fractionated directly (for proteome measurement) and then both were measured by LC-MS/MS. (*D*) Proteome measurements. Left, total number of proteins identified and quantified in the five CTRL and five HF samples. The number quantified in each sample is given. Right, two-dimensional principal component analysis of all samples showing a clear distinction between CTRL and HF samples along the first principal component. (*E* and *F*) Functional enrichment analysis of significantly down-regulated proteins (*E*) and significantly up-regulated proteins (*F*). Similar gene ontology biological process (GO BP) terms were grouped as indicated by the different colours in the pie chart and one representative term of each group is shown. The full lists of terms can be found in Supplementary material online, *Figure S3*. (*G*) Phosphoproteome measurements. Left, total number of phosphorylation events identified and quantified in the five CTRL and five HF samples. The number quantified in each sample is given. Right, two-dimensional principal component analysis of all samples showing a clear distinction between CTRL and HF samples along the first principal component.

Eight weeks post-surgery, the sinus node was isolated (see Supplementary material online, *Figure S2*) and proteins were extracted, digested and isobarically labelled using tandem mass tags (TMT). Combined peptide samples for proteome measurements were fractionated into 38 fractions and samples enriched for phosphorylated peptides were fractionated into 12 fractions by micro-flow reverse-phase ultra-high-pressure liquid chromatography prior to measurement by high-resolution mass spectrometry (*Figure 1C*). We identified 6849 proteins with highly reproducible measurements across biological replicates (Pearson correlation coefficients > 0.98; Supplementary material online, *Figure S3A*). From the proteome data, protein abundances of 6406 proteins were quantified across all samples (*Figure 1D*; Supplementary material online, *Table S1*). Principal component analysis showed a clear distinction between sinus nodes from CTRL and HF mice along the first principal component (*Figure 1D*). Gene Ontology (GO) enrichment analysis showed that proteins with decreased abundances in HF were predominantly involved in cardiac contraction and conduction (*Figure 1E*; Supplementary material online, *Figure S4*), whereas proteins with increased abundances pointed to an immune system response (*Figure 1F*; Supplementary material online, *Figure S4*).

From the samples enriched for phosphorylated peptides, we quantified 6286 phosphorylation events (*Figure 1G*; Supplementary material online, *Table S2*). Again, intensity measurements were highly reproducible (Pearson correlation coefficients ≥ 0.92; Supplementary material online, *Figure S3B*) and there was almost complete overlap of sites measured across all samples (>99%). Principal component analysis of measured intensities for phosphorylated peptides also separated sinus node samples from CTRL and HF animals along the first component (*Figure 1G*). To evaluate phosphorylation signalling differences between CTRL and HF animals, we first had to adjust for the protein remodelling between the two groups. Accordingly, we normalized phosphorylation abundance changes by protein abundance changes (see Supplementary material online, *Figure S3C*). After adjustment for protein regulation, 328 phosphorylation events were up-regulated in HF and 258 were down-regulated (see Supplementary material online, *Figure S3D*) reflecting substantial signalling remodelling in the sinus node. Functional enrichment analysis of proteins with increased phosphorylation levels in HF highlighted an involvement in heart contraction and conduction (see Supplementary material online, *Figure S4*). Increased phosphorylation on proteins involved in these processes is in contrast to the remodelling identified at the protein level. Thus, proteins involved in conduction and contraction appeared as down-regulated while their phosphorylation status was increased. Kinase substrate enrichment analysis (KSEA),[37] which estimates kinase activity changes based on measured changes in phosphorylation levels of substrates, focusing on the 222 kinases we had measured in the sinus node proteomes, pointed to 11 kinases with predicted increased activities in HF including Csnk2a1 (CK2) known to be involved in cardiac hypertrophy,[38] and Mapk14 and Mapk8 (p38-α and JNK1, respectively), stress response kinases known to participate in the pathological cardiac remodelling, development of HF, and arrhythmia[39,40] (see Supplementary material online, *Figure S3E*). The proteome and phosphoproteome measurements document that there is substantial remodelling in the sinus node in HF. These datasets represent an overview of the remodelling characterizing SND in HF and form the foundation to identify proteins and processes involved in the pathological remodelling. This is pursued in the following sections.

3.2 Sinus node ion channels are down-regulated and coupled to heart rate phenotype

We first set out to identify remodelling that may explain the phenotype. The most prominent phenotype characteristic was bradycardia—the decrease in heart rate (*Figure 1A*). From the functional enrichment analysis, the remodelling underlying decreased heart rate would likely be found among the down-regulated proteins (*Figure 1E*). Differential expression analysis revealed 246 down-regulated sinus node proteins in HF mice (*Figure 2A*). To assess the cell types expressing the down-regulated proteins we intersected the protein regulation data with data from sinus node single-nucleus RNA sequencing (snRNAseq) experiments[32] (see Supplementary material online, *Figure S5A*. This data intersection pointed to down-regulated proteins predominantly being expressed by sinus node myocytes (*Figure 2B*; Supplementary material online, *Figure S5B*). Evaluating the protein identities in particular pointed to ion channels, including the important pacemaker funny channels, Hcn1 and Hcn4. Ion channels were in general down-regulated in HF (*Figure 2C*). The down-regulation of ion channel proteins was greater than that of most other myocyte proteins, which suggests that the change is not merely reflecting a change in cell populations (see Supplementary material online, *Figure S5C*). In *Figure 2C*, we have illustrated the ion channel data as a protein interaction network, where the colour of the inner circle reflects the abundance difference of the channel protein between HF and CTRL mice. The outer circle reflects changes in phosphorylation sites quantified for the channels. It appears that, while ion channel protein abundances were down-regulated, several key ion channels were hyperphosphorylated. For example, Na^+ (Scn5a), Ca^{2+} (Cacna1c, Cacna1d, Cacna1h) and K^+ (Kcnh2, Kcnq1) channels responsible for I_{Na}, $I_{Ca,L}$, $I_{Ca,T}$, $I_{K,r}$, and $I_{K,s}$.

To evaluate the functional impact of the measured ion channel protein changes in the sinus node in HF, we applied a computational modelling approach. We used a biophysically detailed model of the mouse sinus node action potential: the Hu-Zhang model.[42] In this, we incorporated the observed down-regulation of proteins responsible for the ionic currents I_f, I_{Na}, $I_{Ca,L}$, $I_{Ca,T}$, $I_{K,r}$, $I_{K,s}$, $I_{K,ACh}$, I_{NaK}, and I_{GJ} (Hcn1, Hcn4, Scn5a, Cacna1c, Cacna1d, Cacna1h, Kcnh2, Kcnq1, Kcnj3, Kcnj5, Atp1a1, Atp1a2, Atp1a3, Cx43) (see Supplementary material online, *Figure S6*). There were no significant changes in the proteins involved in the Ca^{2+} clock mechanism of pacemaking (Atp2a2, Ryr2, and Slc8a1), thus these proteins were not considered further. Simulated action potentials from sinus node cells corresponding to CTRL and HF conditions are shown in *Figure 2D*. The measured changes in ion channel abundances in HF mice resulted in a decrease in the rate of pacemaker action potentials by ∼21% (from 364 to 286 beats/min). This compares favourably to the 20% decrease in

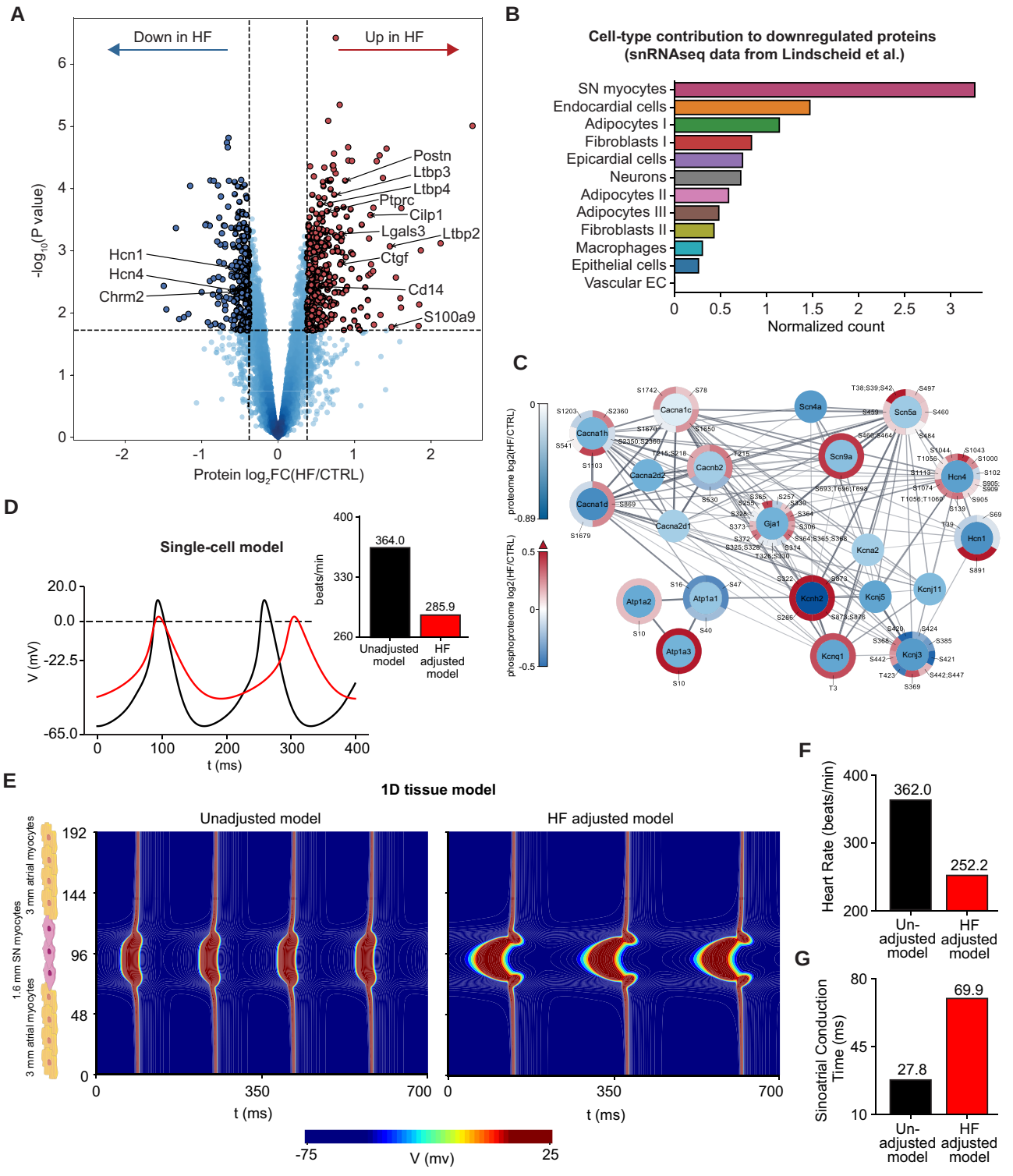

Figure 2 Sinus node ion channel protein expression is reduced and recapitulates reduced heart rate. (*A*) Differential protein expression analysis. Volcano plot shows $\log_2$ transformed fold change of protein abundances in HF compared to CTRL on the *x*-axis and $-\log_{10}$(*t*-test *P*-value) on the *y*-axis. 573 proteins were significantly differentially expressed; 246 proteins were reduced in HF (dark blue dots) whereas 327 proteins were increased (red dots). Proteins with *q*-value < 0.05 (i.e. 5% false discovery rate (FDR), equivalent to $P < 0.019$, indicated by horizontal dashed line) and absolute fold change > 1.3 (indicated by vertical dashed lines) were regarded as significantly differentially expressed. (*B*) Estimated cell type distribution of significantly down-regulated proteins in HF. Estimate is based on proteins with cell-type specific expression evaluated from single-nucleus RNAseq data.[32] The bar chart shows a normalized count per cell type. (*C*) Protein–protein interaction network of ion channel proteins. Nodes reflect proteins; each segment of the outer circle depicts a phosphopeptide identified from that protein. Node colour reflects the logarithmic fold change of protein expression in HF. Colour of the outer circle segments reflects the logarithmic fold change of that phosphopeptide. Thickness of lines between nodes indicates interaction confidence based on STRING DB score.[41]

(continued)

Figure 2 Continued
(*D*) Simulated pacemaking action potentials in the unadjusted (black) and HF adjusted (red) conditions using the Hu-Zhang single-cell model. Graph shows the membrane voltage (mV) over a period of 400 ms. Inset shows the computed heart rate in the unadjusted model and HF adjusted model. (*E*) Simulated initiation and conduction of pacemaking action potentials using a one-dimensional (1D) tissue model of the sinus node and surrounding atrial muscle. Schematic diagram on the left illustrates the model design consisting of 3 mm atrial tissue on either side of 1.6 mm sinus node tissue. The right-hand panels show membrane potential (colour coded) along the length of the model over a period of 700 ms in the unadjusted model (left) and HF adjusted model (right). (*F* and *G*) Computed heart rate (*F*) and computed sinoatrial conduction time (*G*) in the unadjusted model (black) and HF adjusted model (red) from the 1D tissue model.

the beating rate (from 380 to 303 beats/min) of the isolated sinus node from HF mice (*Figure 1B*). To simulate initiation and conduction of pacemaker action potentials, we constructed a one-dimensional model of the sinus node and surrounding atrial muscle (*Figure 2E*). In the sinus node segment, each node (cell) was modelled by the Hu-Zhang model[42] and in the atrial segments each node (cell) was modelled by equations from Aslanidi *et al.*[43] In the control condition, the action potential was initiated in the centre of the sinus node and conducted to the atrial cells in both directions (*Figure 2E*). In the HF condition, although the conduction sequence was not changed, both the pacemaker rate and the conduction of the action potential to the atrial muscle were slowed (*Figure 2F* and *G*) as observed in humans with HF and in the mouse HF model. These results suggest that the reduction in ion channel protein abundance in HF may explain the decreased heart rate in the animal model of HF.

3.3 Multi-modal data integration shortlists seven regulated proteins important for heart rate in humans

In the section above, we present evidence for ion channel down-regulation being a main contributor to the heart rate change in the animal model of HF. To evaluate which of the remodelled proteins in the mouse model are likely to also be important in humans, we intersected the measured proteomics data with matched, orthogonal datasets from humans. The aim was to identify remodelled proteins with evidence from orthogonal human-centric datasets to impact heart rate in humans. First, we intersected all regulated sinus node proteins (*Figure 2A*) and kinases (see Supplementary material online, *Figure S3E*) with genes significantly associated with heart rate. This was based on a genome wide association study (GWAS) performed on 480 000 human subjects identifying 390 loci (see Methods section and Supplementary material online, *Table S3* for details). This data intersection pointed to 48 proteins with regulated abundance being encoded by genes in loci significantly associated with heart rate in humans (*Figure 3A*, HR GWAS panel). Next to the human heart rate GWAS data, the protein abundance changes measured in this study are shown (*Figure 3A*, proteomics panel), as is information on sinus node cell-type expression profile (*Figure 3A*, snRNAseq panel). As seen from the figure, heart rate associated proteins with reduced protein abundances in the HF model were predominantly expressed in sinus node myocytes.

We next asked if any of the 48 proteins, regulated in the mouse model of HF and expressed in a genetic locus associated with heart rate in humans, were targets of drugs reported to cause bradycardia (decreased heart rate) in patients. To this end, we interrogated pharmacovigilance data, focusing on drugs for which bradycardia has been reported as an adverse event and evaluated which on- and off-target proteins interact with these drugs. Accordingly, we queried the *FDA* Adverse Event Reporting System (*FAERS*) database to identify drugs that have a significantly elevated proportion of bradycardia adverse event reports. We employed a multivariable logistic regression model[36] to determine which of these drugs have a significantly elevated odds ratio of bradycardia considering confounders such as sex, age, or other cardiac comorbidities. Twenty-five drugs showed a significantly increased odds ratio for bradycardia (*Figure 3B*). Subsequently, we utilized a drug–gene interaction database to determine protein interactors of each drug[35] and intersected those with the 48 proteins in *Figure 3A*. The drugs with increased odds for bradycardia interact with nine of the 48 shortlisted proteins (*Figure 3B*; Supplementary material online, *Table S4*). We conducted a literature search for each drug–gene interaction to evaluate the evidence and classified them into three categories: strong evidence of interaction (22 drugs with four proteins), medium evidence of interaction (seven drugs with three proteins), and no evidence of interaction (two drugs with two proteins; *Figure 3B*; Supplementary material online, *Table S4*). The latter two were not considered further. Combining the outcome of the pharmacovigilance analysis with the multi-omics data intersection highlighted four proteins with strong evidence of drug–gene interaction, namely Hcn1, Hcn4, Kcnh2, and Chrm2 associated with bradycardia and three proteins with medium evidence of drug–gene interaction, namely Dsp, Cdh2, and Serpine1 associated with bradycardia (*Figure 3A*, FAERS + DGIdb panel).

Taken together, this analysis highlights seven proteins regulated in HF with SND in mice that may have a similar role in humans (Hcn1, Hcn4, Kcnh2, Chrm2, Dsp, Cdh2, Serpine1). Six of these proteins are either ion channels (Hcn1, Hcn4, and Kcnh2) or proteins directly affecting electrical activity (Chrm2, Dsp, and Cdh2). Three of them were already evaluated in the computational modelling in the previous section (Hcn1, Hcn4, Kcnh2). All six proteins are targeted by drugs with increased odds for bradycardia, are predominantly expressed in sinus node myocytes evaluated by snRNAseq data, and had decreased protein abundances in the HF model. We confirmed by genetic knockout experiments that these proteins are important for setting the heart rate (*Figure 3C*). We performed the latter evaluations in zebrafish because gene knockout experiments on zebrafish are rapid, and the electrophysiology of the zebrafish heart holds a significant similarity to that of higher mammals. We did not evaluate the functional consequences of eliminating Hcn1 and Hcn4, as they have both been investigated extensively by others and shown to significantly reduce the heart rate[44–46] In conclusion, the integration of the mouse protein remodelling data with complimentary human datasets once again highlights proteins involved in electrical activity.

3.4 Sinus node inflammation in HF is dominated by macrophage expansion

An important unknown is the identity of the driver of the remodelling, i.e. the immediate cause of SND in HF. To address this, we focused our attention on the parts of the sinus node protein landscape that was up-regulated in HF. Functional enrichment analysis across all proteins with increased abundances pointed to an immune system response (*Figure 1F*). Inflammation-related proteins were significantly more abundant in HF, but their phosphorylation status was not changed (see Supplementary material online, *Figure S7*). Evaluation of the distribution of protein fold changes per cell type suggested an expansion of the macrophage population in the HF animals (see Supplementary material online, *Figure S5C*).

To investigate whether this is also the case for the human, post-mortem samples of the human sinus node were collected. The proteome of the sinus node of human subjects with HF as the basic cause of death and human subjects without heart failure were compared. We evaluated the fold changes of macrophage proteins and found that the majority showed increased abundance in the sinus node of human failing vs. non-failing hearts (51 out of 63; *Figure 4A* and Supplementary material online, *Table S6*). The distribution of fold changes of macrophage proteins was significantly right-shifted ($P = 6.64E^{-10}$; *Figure 4A*) indicating an increase of the macrophage population compared to that of other cell types. These results support expansion of the macrophage population in the sinus node in the human in HF as observed in the mouse.

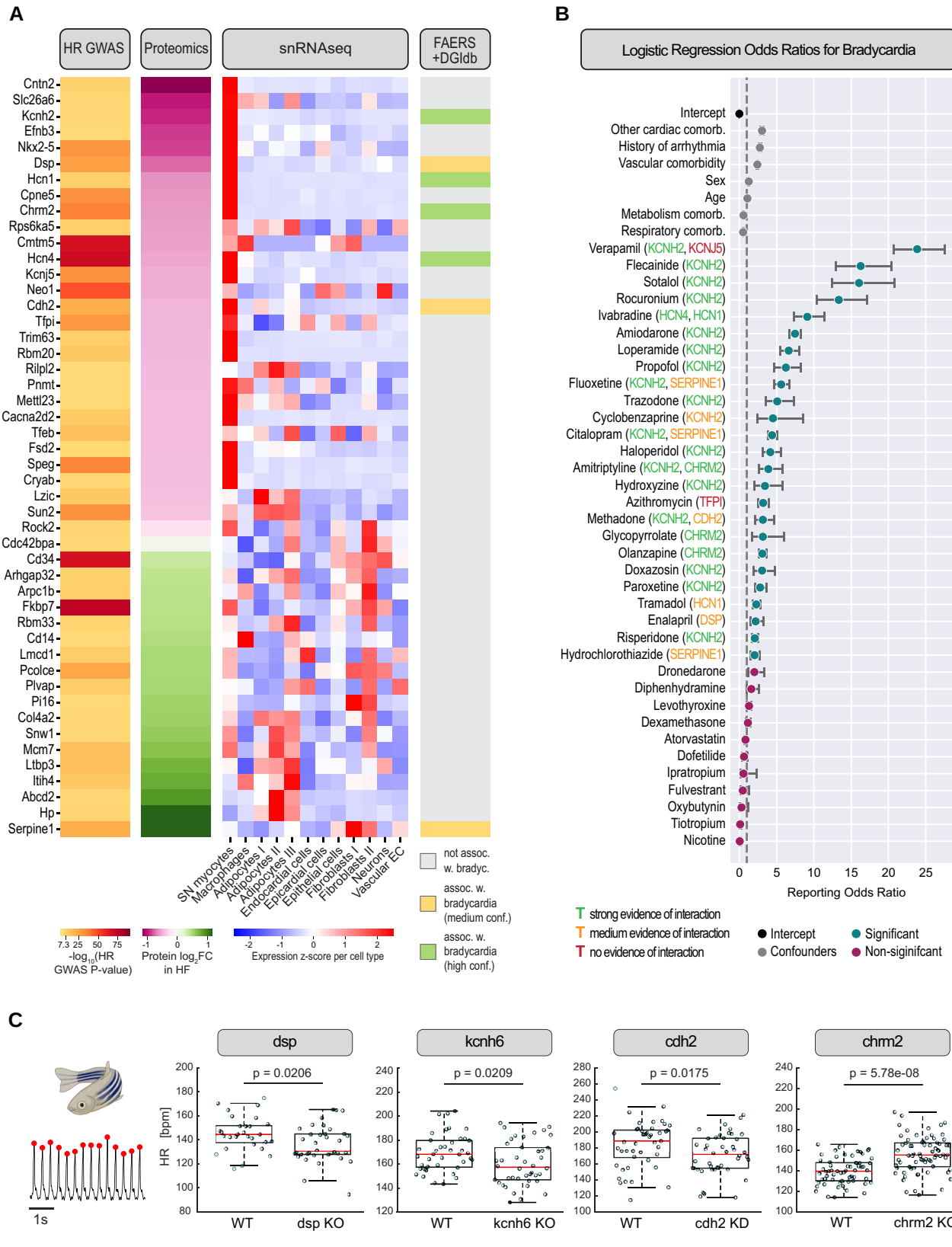

Figure 3 Pharmacovigilance analysis and multi-omics data integration highlights proteins linked to bradycardic phenotype in humans. (*A*) Proteins significantly differentially expressed in the mouse HF with SND model which are also significantly associated with heart rate based on a resting heart rate GWAS of the UK Biobank data. HR GWAS panel, colour corresponds to the $-\log_{10}$(GWAS *P*-value). Proteome panel, colour corresponds to logarithmic fold change of a protein as measured in this study. snRNAseq panel, colour corresponds to the z-scored mRNA expression value of a protein across sinus node cell populations. FAERS + DGIdb panel, colour (green and yellow) indicates association with bradycardia based on *FDA* Adverse Event Reporting System (FAERS) and the (continued)

Figure 3 Continued
drug–gene interaction database (DGIdb) with strong (green) or medium (yellow) evidence of drug–gene interaction. (*B*) Logistic regression analysis of odds ratios for drugs with bradycardia reported as adverse event. Black dot, intercept; grey dots, confounders; turquoise dots, significantly elevated odds ratio; purple dots, non-significant odds ratios. Text colour of gene names indicates level of evidence of the interaction between drug and protein based on literature. Green, strong evidence; yellow, medium evidence; red, no evidence (see also Supplementary material online, *Table S3*). (*C*) Functional evaluation of heart rate (in beats/min, bpm) after gene knockout in zebrafish. Movies of the cardiac cycle were acquired from 10 dpf transparent embryos, from which a signal encoding motion due to chamber contraction was extracted and signal peaks corresponding to individual contractions identified (exemplar, left). Boxes indicate inter-quartile ranges, red lines indicate medians and whiskers show most extreme data out to 1.5× inter-quartile range. Points in the boxplots correspond to individual zebrafish embryos. *P*-values are shown (Mann–Whitney *U* test). Compared to control siblings (WT), knockout of Dsp, Kcnh6 (zebrafish cardiac functional corollary of Kcnh2) and Cdh2 led to a reduced heart rate, whereas knockout of Chrm2 lead to an increased heart rate.

Focusing on the inflammatory response in the mouse model studied, we sought to couple the inflammatory response to a particular cell population. Intersecting the up-regulated proteins with a sinus node snRNAseq dataset suggested that the up-regulated proteins were predominantly expressed by macrophages (*Figure 4B*, Supplementary material online, *Figure S8A*). To evaluate the inflammatory cells further, we utilised a scRNAseq dataset focused on immune cell populations present in the working myocardium in failing mouse hearts.[34] Intersecting the up-regulated proteins with this dataset confirmed that macrophages were the predominant leucocyte population, and in particular Oncostatin-M positive (Osm^+) M1-like macrophages as well as major histocompatibility complex class II positive (MHC-II^+) resident macrophages (*Figure 4C*, Supplementary material online, *Figure S8B*). Whereas a large body of experimental and clinical studies links inflammation to the pathogenesis of HF,[47] such studies have not extended to the sinus node. To bridge this important knowledge gap, we queried the cellular profile involved in the immune response further. Immunolabelling for the pan-macrophage marker IBA-1 confirmed significantly increased numbers of macrophages in the sinus node in HF (*Figure 4D*). We tested whether there was altered expression of MHC-II^+ and C-C chemokine receptor type 2 positive ($CCR2^+$) macrophage subtypes that have been previously shown to be involved in remodelling following HF induced by TAC.[48] Immunolabelling experiments showed significantly greater levels of both MHC-II and CCR2 in the sinus node in HF (*Figure 4E* and *F*). In conclusion, our results demonstrate an immune response, and in particular an increased macrophage presence, in the sinus node in the mouse TAC model of HF.

3.5 Sinus node inflammation can affect electrical homeostasis

We sought to assess the functional significance of local inflammation and macrophage activation on sinus node function. To this end, sinus node preparations from mice were cultured in the presence of lipopolysaccharide (LPS), a potent stimulant of macrophages that acts via Toll-like receptor 4.[49] Sinus node preparations were incubated for 24 h in the presence or absence of LPS using a previously established method.[50] After incubation with LPS, as expected, there was evidence of a local pro-inflammatory response: an up-regulation of galectin-3 (Lgals3) protein, a 30 kDa β-galactoside-binding lectin and an inflammatory marker, as measured by western blot (*Figure 5A*, Supplementary material online, *Figure S9*) and an up-regulation in transcripts for two master pro-inflammatory cytokines, tumour necrosis factor alpha (Tnf) and interleukin-1 beta (Il1b), measured by qPCR (*Figure 5B*). As already shown (*Figure 2A*, Lgals3), in the sinus node in HF galectin-3 protein was also up-regulated (to 177% of CTRL); it is a challenge to detect low abundance cytokines by mass spectrometry and Tnf and Il1b were not detected in this study. After incubation with LPS, there was a down-regulation of Hcn4 transcript (*Figure 5C*) as there was in the case of Hcn4 protein in the sinus node in HF (*Figure 2A*). Finally, intracellular recording of pacemaker action potentials by sharp microelectrodes showed that incubation with LPS resulted in a slowing of the intrinsic pacemaker activity of the sinus node, i.e. an increase of the cycle length (*Figure 5D* and *E*, Supplementary material online, *Figure S9*); this is equivalent to the decrease of the intrinsic heart rate in HF (*Figure 1B*). Spontaneous early afterdepolarisations were also observed in the sinus node incubated with LPS (*Figure 5D*). These data show that local inflammation in the sinus node has direct functional consequences for sinus node electrical activity.

3.6 Targeting pro-inflammatory galectin-3 signalling ameliorates SND in HF

The results presented above suggest a novel mechanism linking inflammation and electrical activity of the sinus node. Therefore, modulation of the inflammatory response may present a potential strategy to mitigate SND in HF. We thus evaluated all the regulated inflammatory proteins in the proteomics data for a potential therapeutic target and ultimately decided on galectin-3 (see *Figure 2A*). Galectin-3 is a pro-inflammatory protein expressed and secreted by macrophages[51] and has emerged as an important regulator of pathophysiological remodelling in HF.[52–54] We hypothesized that inhibition of galectin-3 may prevent or delay the onset of SND in HF.

To test this, we randomised CTRL and HF animals into anti-galectin-3 treated and untreated groups. Animals in the anti-galectin-3 treated group received MCP, a complex water-soluble indigestible polysaccharide rich in β-galactose, shown to be effective in suppressing circulating and cardiac tissue levels of galectin-3.[55] Mice in the treatment group were dosed starting from the day of surgery and continuing until the experimental endpoint (*Figure 6A*). We verified that treatment was effective by assessing sinus node protein expression levels of fumarate hydratase (see Supplementary material online, *Figure S10*), natively down-regulated by galectin-3[56] and recently used to confirm the efficacy of MCP dosing in drinking water.[57] Immunolabelling for the pan-macrophage marker IBA-1 demonstrated that the significant expansion of macrophages in the sinus nodes in HF was partly mitigated by MCP treatment (see Supplementary material online, *Figure S11*).

The heart rate, measured *in vivo* in conscious and unrestrained mice on the day of termination, demonstrated that MCP treatment blunted the heart rate reduction seen in the untreated HF animals (*Figure 6B*)—whereas there was a significant reduction in heart rate of HF animals receiving vehicle, this heart rate difference was no longer apparent between the groups receiving MCP treatment. This was also reflected in a reduction in heart rate difference in consequence to HF for the animals receiving MCP treatment compared to those that received vehicle (*Figure 6B*, right). To evaluate intrinsic heart rate, high resolution unipolar multielectrode array mapping (500 μm interelectrode distance) of the electrical activity was carried out on the endocardial surface of isolated sinus node preparations from the four groups of animals. The intrinsic heart rate was significantly reduced consequent to HF in animals receiving vehicle, but this reduction was mitigated in MCP-treated HF animals (*Figure 6C*, left). Similarly, prolongation of the cSNRT seen in untreated HF animals was absent in HF animals receiving MCP (*Figure 6C*, right).

Analysis of activation maps demonstrated that HF hearts had an inferior leading pacemaker site as well as slower sinoatrial conduction than CTRL animals, which had a leading pacemaker site in the superior intercaval

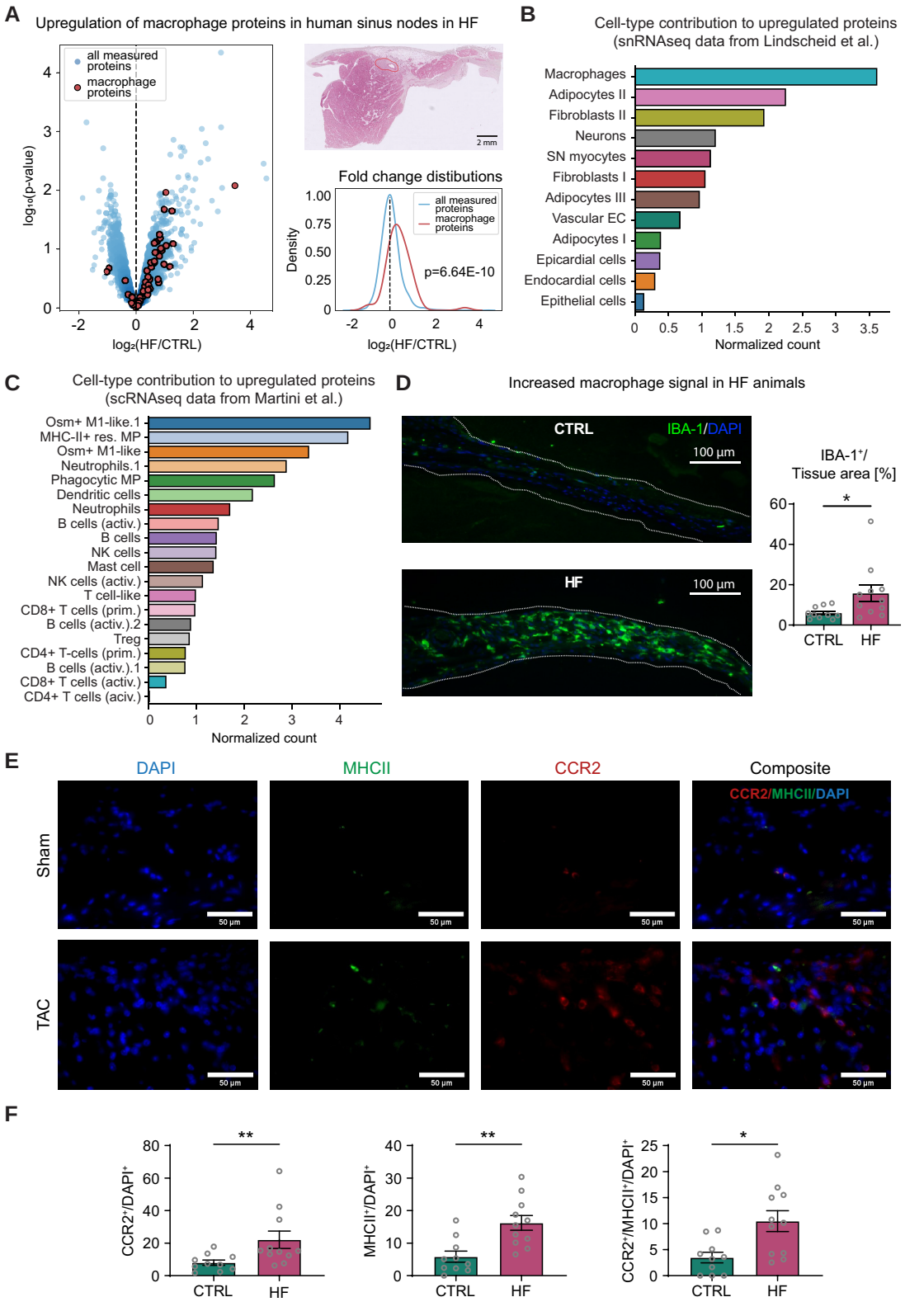

Figure 4 Linking local inflammation and macrophage expansion with SND in HF. (*A*) Sinus node proteome measurements from human subjects with HF as the cause of death ($n = 4$) and human subjects without HF ($n = 3$). Left, volcano plot shows $\log_2$ transformed fold change of sinus node protein abundance in the diseased vs. control condition on the *x*-axis and the $-\log_{10}$(*t*-test *P*-value) on the *y*-axis. Red dots indicate proteins that are predominantly expressed by macrophages based on human and mouse snRNAseq data. 51/63 macrophage proteins showed increased abundance in human HF sinus nodes. Top right, representative H&E stain of human atrial tissue section. Sinus node outlined in red. Scale bar 2 mm. Bottom right, distribution of fold changes of macrophage proteins is significantly shifted to the right compared to the fold change distribution of all quantified proteins. *P*-value shown (Mann–Whitney *U* test).
(continued)

Figure 4 Continued

(*B*) Estimated cell type contribution for significantly up-regulated proteins in HF mice. Estimate is based on proteins with cell-type specific expression evaluated from single-nucleus RNAseq data from murine sinus node.[32] The bar chart shows the normalized count of proteins for each cell type. (*C*) Same as panel *B*, but based on scRNAseq data from Martini *et al.*[34] (*D*) Immunolabelling of the pan-macrophage marker IBA-1. Left, representative immunolabelling of IBA-1 (green signal) and DAPI (nuclear marker; blue signal) in sinus node preparations of CTRL and HF animals. The sinus node is outlined by the white dotted lines. Scale bar, 100 μm. Right, expression of IBA-1. The mean ± S.E.M. (as well as individual data points) percentage of IBA-1 positive pixels per sinus node tissue area in sinus node preparations from CTRL and HF animals is plotted ($n = 10/11$ sections taken at 200 μM intervals of the intercaval region from three animals per group). *$P < 0.05$ (Mann–Whitney *U* test). (*E*) Representative DAPI (nuclear stain), CCR2 and MHC-II immunolabelling (and composite image) of sinus nodes from sham-operated and TAC mice. Scale bar = 50 μm. (*F*) Summary data derived from images such as those in the top panel showing $CCR2^+$ and $MHC\text{-}II^+$ immunolabelling (plus the sum of the two) as a percentage of the DAPI signal. ~11 slides from three mice animals per group were analysed. Means ± S.E.M. as well as individual data points shown. *$P < 0.05$, **$P < 0.01$ (Mann–Whitney *U* test, $n = 10/11$).

region near the opening of the superior vena cava and faster sinoatrial conduction (*Figure 6D*; Supplementary material online, *Figure S12*). The HF-induced changes to the leading pacemaker site and sinoatrial conduction were abrogated by MCP treatment (*Figure 6D*; Supplementary material online, *Figure S12*). Unipolar fractionated electrograms—indicative of structural and electrical remodelling resulting in asynchronous activation of myocytes[58]—were significantly more prevalent in untreated HF animals (*Figure 6E*). The incidence of complex fractionated electrograms was restored to CTRL levels in the HF group receiving MCP treatment (*Figure 6E*; Supplementary material online, *Figure S12*). Taken together, these studies show that early and sustained pro-inflammatory galectin-3 suppression is effective in preventing SND in HF.

Galectin-3 suppression ameliorated HF in other ways as well: as expected, left ventricular functional parameters—ejection fraction and GLS—were significantly worse in HF in untreated animals. However, in HF, the decrease in ejection fraction was partially mitigated and the decrease in GLS was no longer significant in the MCP-treated group (*Figure 6F* and *G*). MCP treatment altered the heart failure phenotype: in HF, whereas the left ventricle internal diastolic diameter and end-diastolic volume were significantly increased in untreated animals, these parameters were restored to control levels in the MCP-treated group (*Figure 6H* and *I*). Instead, in HF, MCP-treated animals presented with a significant increase in the left ventricle relative wall thickness (*Figure 6J* and *K*). These findings indicate that MCP treatment delayed the transition from a hypertrophic to a dilated cardiomyopathy.

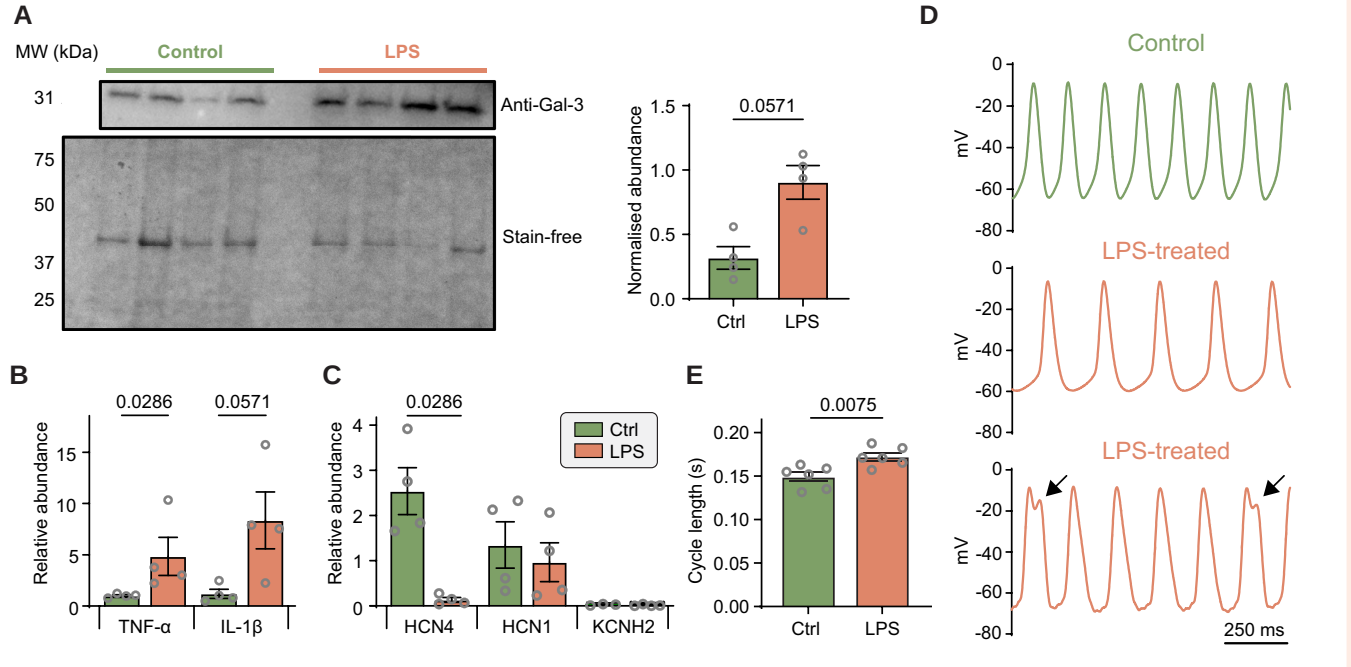

Figure 5 Linking local inflammation to electrical remodelling. (*A*, left) Representative Galectin-3 western blot of sinus node biopsies SAN explants incubated in the absence (control) or presence (LPS) of 1 μg/mL LPS. Corresponding stain-free total protein gel used for quantification is shown in the lower panel. Right, Mean ± S.E.M. (as well as individual data points) galectin-3 protein expression (quantified by western blot) in sinus node preparations incubated in the absence (control) or presence (LPS) of 1 μg/mL LPS. *P*-value shown (Mann–Whitney *U* test; $n = 4/4$). (*B*) Mean ± S.E.M. (as well as individual data points) expression of *TNF*-α and interleukin-1β mRNA (normalised to the expression of Ipo8 and 18 s) in sinus node preparations incubated in the absence (control, green) or presence (LPS, orange) of 1 μg/mL LPS. *P*-values shown (Mann–Whitney *U* test; $n = 4/4/4/4$). (*C*) Mean ± S.E.M. (as well as individual data points) expression of pacemaker ion channel mRNAs (Hcn1, Hcn4, and Kcnh2; to the expression of Ipo8 and 18 s) in sinus node preparations incubated in the absence (control, green) or presence (LPS, orange) of 1 μg/mL LPS. *P*-value shown (Mann–Whitney *U* test; $n = 4/4/4/4/3/4$). (*D*) Representative intracellular action potentials recorded from mouse sinus node preparations cultured for 24 h in the absence (control) or presence (LPS) of 1 μg/mL LPS. Cycle lengths: top = 140 ms, middle = 210 ms, bottom = 165 ms. Arrows indicate early afterdepolarisations observed only in LPS treated preparations. (*E*) Mean ± S.E.M. (as well as individual data points) spontaneous cycle length measured in experiments like those in panel *D*. *P*-value shown (Mann–Whitney *U* test; $n = 6/6$).

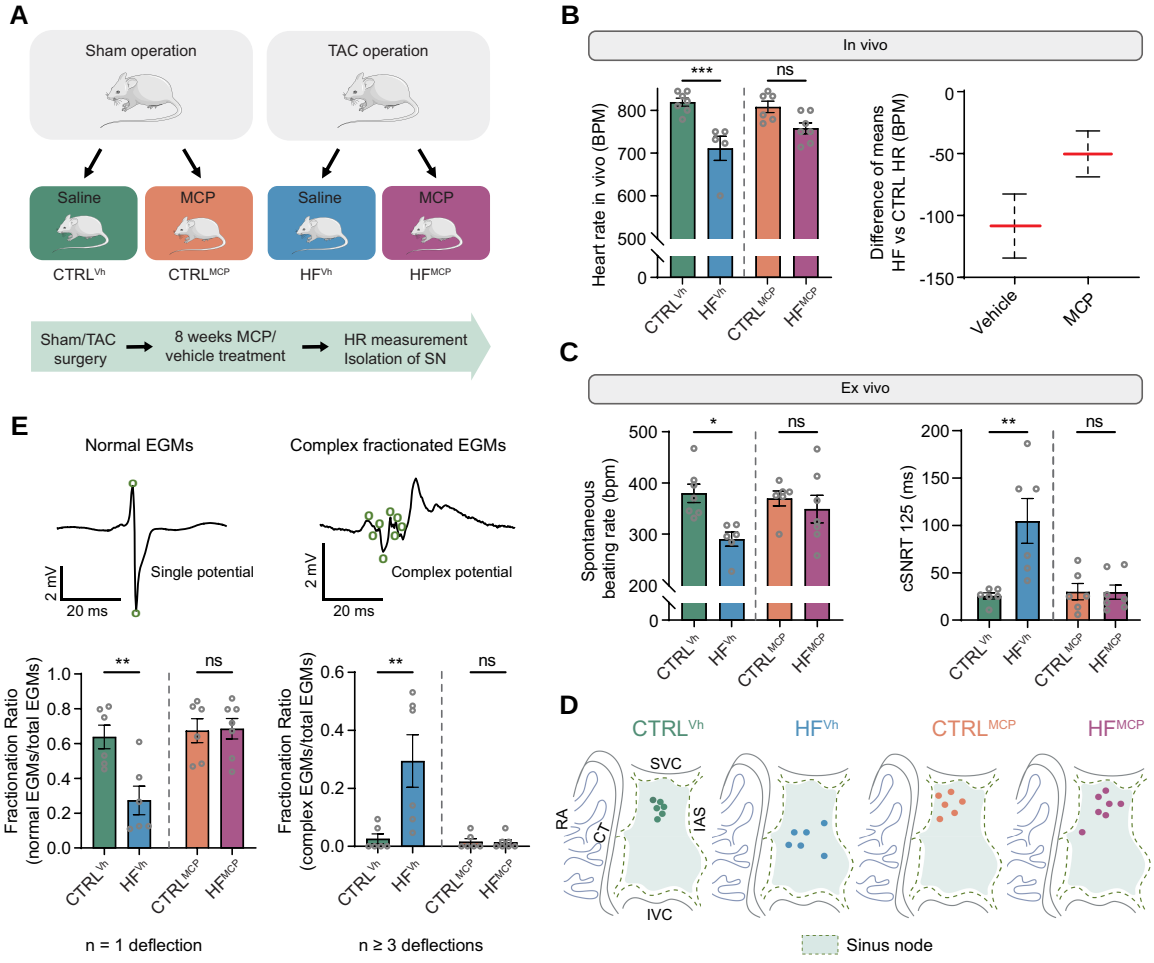

Figure 6 Targeting galectin-3 signalling prevents SND in HF. (*A*) Experimental design for evaluating prevention of SND in TAC-induced HF by systemic galectin-3 targeting with MCP. (*B*) Effect of MCP treatment on the change in heart rate *in vivo* in HF. Left, mean ± S.E.M. (as well as individual data points) heart rate (measured in conscious animals on day of termination) in vehicle-treated and MCP-treated CTRL and HF mice ($n = 7/5/6/7$). ***$P < 0.001$ (two-way ANOVA with Tukey's multiple comparisons test); ns, not significant. Right: difference in heart rate between HF and CTRL mice receiving vehicle treatment and the difference in heart rate between HF and CTRL animals receiving MCP. (*C*) Effect of MCP treatment on the change in function of the isolated sinus node in HF. The spontaneous beating rate (in beats/min, bpm, $n = 7/6/6/7$) and the corrected sinus node recovery time (cSNRT, $n = 6/6/6/7$) after stimulation at a cycle length of 125 ms are shown in vehicle-treated and MCP-treated CTRL and HF mice. *$P < 0.05$ (two-way ANOVA with Tukey's multiple comparisons

(continued)

Figure 6 Continued
test); ns, not significant. The spontaneous beating rate and cSNRT in vehicle-treated CTRL and HF animals are reproduced from *Figure 1B*. (*D*) Effect of MCP treatment on the change in the position of the leading pacemaker site in HF. Points show the estimated position of the leading pacemaker site in vehicle-treated and MCP-treated CTRL and HF mice ($n = 6/6/6/7$). The position of the leading pacemaker site was derived from activation maps such as those shown in Supplementary material online, *Figure S12*. (*E*) Effect of MCP treatment on electrogram (EGM) fractionation. Top, representative EGMs illustrating a normal EGM and a complex fractionated EGM. A unipolar EGM recorded at a site where an activation front passes the electrode results in a biphasic deflection (marked by green circles). Bottom, mean ± S.E.M. (as well as individual data points) fractionation ratio given as number of normal (left) or complex fractionated (right) EGMs compared to the total number of EGMs in vehicle-treated and MCP-treated CTRL and HF mice ($n = 6/6/6/7$). $^{**}P < 0.01$ (two-way ANOVA with Tukey's multiple comparisons test); ns, not significant. (*F*) Representative B-mode echocardiographic images taken in end diastole in parasternal long-axis view. Red traces indicate the endocardial border and yellow traces the epicardial border. (*G–K*) Effect of MCP treatment on the changes in heart function in HF. Mean ± S.E.M. (as well as individual data points, $n = 6/5/7/6$) ejection fraction (*G*), global longitudinal strain (GLS, *H*), left ventricle internal diastolic diameter (LVIDd, *I*), left ventricle end-diastolic volume (*J*), and left ventricle relative wall thickness (*K*) are shown in untreated (control) and MCP-treated sham-operated and TAC mice. $^{*}P < 0.05$, $^{**}P < 0.01$, $^{***}P < 0.001$, $^{****}P < 0.0001$ (two-way ANOVA followed by Tukey's multiple comparisons test).

4. Discussion

In this study, we investigated protein remodelling of the sinus node in an animal model of HF and concurrent SND. Our evaluation of sinus node protein remodelling was based on quantitative information from 6406 proteins. Pursuing a data-driven strategy to shortlist remodelling of likely relevance also for SND in humans, we intersected the proteome remodelling data with human GWAS data on heart rate. This highlighted 48 proteins, several of which are well known for their impact on heart rate, whereas others are less studied in this context. For some of the less studied proteins, there is evidence from animal models that they may indeed influence heart rate, e.g. reduced abundance of Slc26a6 (responsible for an electrogenic Cl^-/HCO_3^- exchanger in the heart) causes sinus bradycardia in mice.[59] To further prioritize among the 48 shortlisted proteins, we focused on those that interact with drugs with significantly elevated odds ratio of bradycardia as a reported side effect. Of these, three proteins are ion channels (Hcn1, Hcn4, and Kcnh2), a receptor (Chrm2), two intercalated disc proteins involved in myocyte coupling (Cdh2 and Dsp), and a fibroblast protein involved in the pathophysiology of fibrosis (Serpine1). Here, we focused on the six proteins coupled to electrical homeostasis. The presence of Hcn1, Hcn4, and Kcnh2 in this list is not a surprise: we showed that knockdown of the Kcnh2 functional corollary in zebrafish caused bradycardia and other independent studies have shown that knockout or inhibition of these channels causes a decrease in sinus node pacemaking.[44–46,60] Furthermore, all three channels were included in the computer modelling that predicted sinus bradycardia consequent to the measured ion channel down-regulation. Down-regulation of ion channels in the sinus node of failing hearts is consistent with previous studies.[11,25,26,61,62] The presence of intercalated disc proteins (Cdh2 and Dsp) is also in line with current understanding. The intercalated disc plays a central role in the transmission of force, action potential conduction and chemical communication between cardiomyocytes and has been strongly implicated in HF.[63] Conditional knockout of Cdh2 in mice has been reported to reduce heart rate and slow conduction[64,65] and absence of Dsp in the sinus node has been shown to cause sinus pauses and dysfunction.[66] We further strengthened the experimental support for both proteins: knockdown of the two proteins in zebrafish resulted in reduced heart rates. Down-regulation of the cardiac ACh receptor (Chrm2) in a heart failure with bradycardia model is counterintuitive, as Chrm2 loss would be expected to increase resting heart rate, as confirmed by knockout in zebrafish. However, down-regulation of Chrm2 may be part of the decline in vagal control and concurrent *elevated* resting heart rates observed in *early* stages of heart failure.[67] In summary, (i) the proteomics showing a down-regulation of proteins related to electrical activity in HF, (ii) the data-driven strategy to shortlist HF-remodelled proteins likely to impact heart rate, (iii) the effect on heart rate of knockout of HF-remodelled ion channels in the zebrafish, and (iv) computer modelling of sinus node electrical activity incorporating the observed down-regulation of ion channel proteins in HF shows that the remodelling of ion channels likely underlies the SND in HF.

Utilising the information in the proteomics dataset, we addressed the trigger of sinus node remodelling changes in HF. We were intrigued to find that the predominant signal among up-regulated proteins came from an inflammatory response, which in particular pointed to an expansion of the macrophage population. We confirmed this by classical immunolabelling. In the working myocardium, the role of inflammation in HF pathogenesis is well established, and dynamic interplay between inflammation and fibrosis with activation of the innate and adaptive immune systems has been described.[47,68–71] For example, Martini *et al.*[34] showed that the working myocardium in HF is characterized by recruitment of diverse immune cell populations, notably M1-like $CCR2^+$ Osm^+ $Il1b^+$ macrophage populations. Lavine *et al.*[72] has reported that the non-failing mouse heart contains two resident macrophage ($MHC\text{-}II^{low}CCR2-$, $MHC-II^{high}CCR2-$) subsets and one monocyte-derived macrophage ($MHC\text{-}II^{high}CCR2+$) subset and, post-injury, there is recruitment of $MHC\text{-}II^{high}CCR2+$ monocyte-derived macrophages.[72] Furthermore, Patel *et al.*[48] have reported that, in the mouse TAC model, there is an ~8-fold increase in $CCR2^+$ macrophages, and this is responsible for adverse cardiac remodelling and the transition to HF. In a mouse myocardial infarction model of HF, macrophage expansion in the non-ischaemic remote zone has been attributed to recruitment of monocyte-derived macrophages driven by increased expression of cell adhesion molecules responsible for leucocyte trafficking: intercellular adhesion molecule 1 (Icam1), vascular cell adhesion molecule 1 (Vcam1) and E- and P-selectin; their silencing *in vivo* curbed monocyte recruitment and preserved the ejection fraction.[73] In the sinus node of the HF mice, all four identified adhesion molecules were up-regulated (see Supplementary material online, *Figure S7C*), and we observed increased levels of MHC-II and CCR2+ macrophages suggesting a similar mechanism in the sinus node.

Furthermore, we addressed the functional link between inflammation, specifically macrophage activation, and the electrical properties of the sinus node. We report that exposure of isolated sinus node preparations to LPS, which activates macrophages via Tlr4 signalling,[49] and leads to an increase in protein abundance of galectin-3, results in a down-regulation of Hcn4 and a slowing sinus node pacemaking. This is plausible—it is known that LPS-induced changes in pro-inflammatory cytokines result in changes in cardiac ion channel expression and function.[74]

Having observed a functional coupling between sinus node inflammation and electrical remodelling, the question that immediately presents is whether modulation of the macrophage-mediated inflammatory response could mitigate SND. As a first step, we adopted a loss-of-function approach centred on galectin-3 as it co-localises with activated macrophages in the heart[75,76] and mediates pro-inflammatory and profibrotic processes.[55,77,78] Furthermore, up-regulation of galectin-3 has been demonstrated in failing human hearts,[75] and prognostic studies show that an increased circulating level of galectin-3 is an independent predictor of

adverse cardiovascular outcomes in both acute and chronic HF.[79,80] Our finding that systemic galectin-3 inhibition in HF blunts the decrease in the normal heart rate *in vivo*, abolishes the decrease of the intrinsic heart rate, abolishes the increase in the sinus node recovery time, restores the leading pacemaker site to a superior region, and likely prevents structural changes that result in fractionated electrograms, establishes a direct link between inflammation and SND in HF. The shift of the leading pacemaker site in the sinus node is common and occurs in response to many interventions; in humans, it is referred to as the 'wandering pacemaker'.[81] Pacemaker shift is a consequence of the heterogeneity of the sinus node—the electrophysiology of the sinus node varies from the centre to the periphery of the node as well as from the superior to the inferior extent of the node[81] likely as a result of regional differences in ion channel expression and ionic current densities.[81,82]

Our findings of beneficial effects on sinus node function of systemic galectin-3 inhibition are in line with previous work showing that galectin-3 inhibition by systemic delivery of MCP, as performed in this study, suppresses inflammation and prevents structural remodelling in animal models of HF including myocardial infarction,[57] aortic stenosis,[83] isoproterenol-induced HF,[55] obesity-related cardiomyopathy,[84] and hyperaldosteronism[77]; in this study, galectin-3 inhibition also suppressed structural remodelling (*Figure 6F–K*). Furthermore, Takemoto *et al.*[85] demonstrated that $I_{K,ur}$ remodelling in a sheep model of atrial fibrillation could be abrogated by treatment with galactomannan, which inhibits galectin-3 akin to the mode of action of MCP. Galectin-3 inhibition could be a potential therapy for SND in HF. However, further focused studies on understanding the involvement of macrophages and galectin-3 in nodal pathophysiology in large animal models of HF and in human patients are critical in determining potential translational value. For example, it cannot be ruled out that the effects of galectin-3 inhibition on the sinus node are secondary to the reduction in structural remodelling rather than a direct effect of the sinus node.

In conclusion, this study demonstrates that SND in HF is the likely consequence of a down-regulation of proteins involved in the electrical activity in the sinus node, but importantly, this study also directly links macrophage expansion to the molecular remodelling that underlies SND in HF. Local inflammation in general and galectin-3 signalling in particular present a novel target to treat SND in HF.

Limitations of the study are discussed in the Supplementary material.

Translational perspective

Heart failure patients with sinus node dysfunction (SND) face an increased risk of mortality, yet the underlying molecular mechanisms are poorly understood. This study reveals extensive protein and phosphorylation remodelling in the sinus node in mice with heart failure and SND. We highlight down-regulation of specific ion channels as key contributors and utilise multi-omics data integration to pinpoint protein dysregulation likely relevant to SND in humans. Additionally, our data suggest inflammation as a driver of electrophysiological remodelling and identify galectin-3 as a potential therapeutic target. These findings offer insight into the molecular basis of SND in heart failure and could facilitate the development of new therapies.

Supplementary material

Supplementary material is available at *Cardiovascular Research* online.

Authors' contributions

Animal surgery (M.Z.); physiological measurements, isolation of sinus nodes, and statistical analysis of animal work (C.W., L.S., M.S., A.D.); MCP dosing (M.S., A.D.); *ex vivo* electrophysiology, histology, imaging, macrophage labelling, and analysis in mice (L.S., A.D.); sample preparation, phosphopeptide enrichment, and mass spectrometry measurements (S.M.); human samples and immunostaining (T.H.L.J., K.B.O., J.J.); MS data processing and analysis (K.K.); bioinformatic data analyses (K.K.); GWAS analysis (Y.J.v.d.V., K.K., P.v.d.H.); mathematical modelling of the sinus node (W.H., H.Z.); drug-target analysis and mathematical modelling (F.B.H., R.W.M.); zebrafish knock-downs and heart rate measurements (R.W.M.); genomic data sources (M.S.O.); conceptualization of project (M.R.B., A.D., A.L.); project lead (K.K.); project supervision (M.R.B., A.D., A.L.); interpretation of data (K.K., A.S., R.W.M., A.D., L.S., M.R.B., A.L.); data visualization (K.K.); writing—original draft (K.K., M.R.B., A.D., A.L.); writing—review and editing (all authors).

Acknowledgements

The authors thank all lab members for fruitful discussions, Nancy Mutsaers for graphical assistance, and Signe Lykke Nielsen for assistance in the zebrafish experiments. Furthermore, we thank all UK Biobank participants for their participation and valuable contributions. This research has been conducted using the UK Biobank Resource under application number 12010. The graphical abstract, *Figure 1C*, *Figure 6A* and Supplementary Figure S5A were partly created by using and/or adapting Servier Medical Art, licensed under CC BY 4.0. *Figure 3C*, *Figure 6D* and Supplementary Figure S12A were partly created with BioRender.com.

Conflict of interest: none declared.

Funding

In Denmark, this work was supported by the Carlsberg Foundation (CF17-0209) and the Novo Nordisk Foundation (NNF20OC0059767) to A.L. The mass spectrometry measurements were performed at the Novo Nordisk Foundation Center for Protein Research, which is funded in part by a generous donation from the Novo Nordisk Foundation (NNF14CC0 001). A.S. was supported by a training grant from the Lundbeck Foundation (R322-2019-2698). Work at the University of Manchester and Imperial College London was supported by a British Heart Foundation Intermediate Fellowship (FS/19/1/34035) and British Heart Foundation Project grant (PG/22/10919) to AD, a British Heart Foundation Programme Grant to M.R.B (RG/18/2/33392) and a Fondation Leducq TNE FANTASY (19CV03) grant to AD and MRB. MS and SA were supported by British Heart Foundation PhD Studentships (FS/18/62/34183, FS/CRTF/23/24469).

Data availability

All mass spectrometry raw data and search results from this study were uploaded to the ProteomeXchange Consortium via the PRIDE repository[86] with the identifier: PXD031084. The data are accessible through https://www.ebi.ac.uk/pride/archive and project name 'Proteomics couples electrical remodelling to inflammation in a murine model of heart failure with sinus node dysfunction'. The GWAS on resting heart rate in the UK Biobank will be part of a large meta-analysis of resting heart rate, which is yet to be published. The full GWAS summary statistics of the UK Biobank will be made available upon publication. The full list of significant genomic risk loci and the genes they were mapped to are available in Supplementary material online, *Table S3* of this publication.

The code of the bioinformatics analyses is provided as Jupyter notebooks in our GitHub repository https://github.com/CardiacProteomics/sinus-node-heart-failure.

References

1. Ambrosy AP, Fonarow GC, Butler J, Chioncel O, Greene SJ, Vaduganathan M, Nodari S, Lam CS, Sato N, Shah AN, Gheorghiade M. The global health and economic burden of hospitalizations for heart failure: lessons learned from hospitalized heart failure registries. *J Am Coll Cardiol* 2014;**63**:1123–1133.
2. GBD 2017 Disease and Injury Incidence and Prevalence Collaborators. Global, regional, and national incidence, prevalence, and years lived with disability for 354 diseases and injuries for 195 countries and territories, 1990–2017: a systematic analysis for the Global Burden of Disease Study 2017. *Lancet* 2018;**392**:1789–1858.
3. Shen L, Jhund PS, Petrie MC, Claggett BL, Barlera S, Cleland JGF, Dargie HJ, Granger CB, Kjekshus J, Køber L, Latini R, Maggioni AP, Packer M, Pitt B, Solomon SD, Swedberg K, Tavazzi L, Wikstrand J, Zannad F, Zile MR, McMurray JJV. Declining risk of sudden death in heart failure. *N Engl J Med* 2017;**377**:41–51.
4. Luu M, Stevenson WG, Stevenson LW, Baron K, Walden J. Diverse mechanisms of unexpected cardiac arrest in advanced heart failure. *Circulation* 1989;**80**:1675–1680.
5. Stevenson WG, Stevenson LW, Middlekauff HR, Saxon LA. Sudden death prevention in patients with advanced ventricular dysfunction. *Circulation* 1993;**88**:2953–2961.
6. Faggiano P, d'Aloia A, Gualeni A, Gardini A, Giordano A. Mechanisms and immediate outcome of in-hospital cardiac arrest in patients with advanced heart failure secondary to ischemic or idiopathic dilated cardiomyopathy. *Am J Cardiol* 2001;**87**:655–651.
7. Gang UJO, Jons C, Jorgensen RM, Abildstrom SZ, Haarbo J, Messier MD, Huikuri HV, Thomsen PEB; CARISMA investigators. Heart rhythm at the time of death documented by an implantable loop recorder. *Europace* 2010;**12**:254–260.
8. Bloch Thomsen PE, Jons C, Raatikainen MJP, Moerch Joergensen R, Hartikainen J, Virtanen V, Boland J, Anttonen O, Gang UJ, Hoest N, Boersma LV, Platou ES, Becker D, Messier MD, Huikuri HV. Long-term recording of cardiac arrhythmias with an implantable cardiac monitor in patients with reduced ejection fraction after acute myocardial infarction: the Cardiac Arrhythmias and Risk Stratification After Acute Myocardial Infarction (CARISMA) study. *Circulation* 2010;**122**:1258–1264.
9. Jose AD, Taylor RR. Autonomic blockade by propranolol and atropine to study intrinsic myocardial function in man. *J Clin Invest* 1969;**48**:2019–2031.
10. Yanni J, Tellez JO, Maczewski M, Mackiewicz U, Beresewicz A, Billeter R, Dobrzynski H, Boyett MR. Changes in ion channel gene expression underlying heart failure-induced sinoatrial node dysfunction. *Circ Heart Fail* 2011;**4**:496–508.
11. Zicha S, Fernandez-Velasco M, Lonardo G, L'Heureux N, Nattel S. Sinus node dysfunction and hyperpolarization-activated (HCN) channel subunit remodeling in a canine heart failure model. *Cardiovasc Res* 2005;**66**:472–481.
12. Opthof T, Coronel R, Rademaker HM, Vermeulen JT, Wilms-Schopman FJ, Janse MJ. Changes in sinus node function in a rabbit model of heart failure with ventricular arrhythmias and sudden death. *Circulation* 2000;**101**:2975–2980.
13. Sanders P, Kistler PM, Morton JB, Spence SJ, Kalman JM. Remodeling of sinus node function in patients with congestive heart failure: reduction in sinus node reserve. *Circulation* 2004;**110**:897–903.
14. Dobrzynski H, Anderson RH, Atkinson A, Borbas Z, D'Souza A, Fraser JF, Inada S, Logantha SJRJ, Monfredi O, Morris GM, Moorman AFM, Nikolaidou T, Schneider H, Szuts V, Temple IP, Yanni J, Boyett MR. Structure, function and clinical relevance of the cardiac conduction system, including the atrioventricular ring and outflow tract tissues. *Pharmacol Therapeut* 2013;**139**:260–288.
15. Dobrzynski H, Boyett MR, Anderson RH. New insights into pacemaker activity: promoting understanding of sick sinus syndrome. *Circulation* 2007;**115**:1921–1932.
16. Chan C-S, Lin Y-K, Chen Y-C, Lu Y-Y, Chen S-A, Chen Y-J. Heart failure differentially modulates natural (sinoatrial node) and ectopic (pulmonary veins) pacemakers: mechanism and therapeutic implication for atrial fibrillation. *Int J Mol Sci* 2019;**20**:3224.
17. Zweerink A, van der Lingen ACJ, Handoko ML, van Rossum AC, Allaart CP. Chronotropic incompetence in chronic heart failure. *Circ Heart Fail* 2018;**11**:e004969.
18. Benes J, Kotrc M, Borlaug BA, Lefflerova K, Jarolim P, Bendlova B, Jabor A, Kautzner J, Melenovsky V. Resting heart rate and heart rate reserve in advanced heart failure have distinct pathophysiologic correlates and prognostic impact: a prospective pilot study. *JACC Heart Fail* 2013;**1**:259–266.
19. Witte KKA, Cleland JGF, Clark AL. Chronic heart failure, chronotropic incompetence, and the effects of beta blockade. *Heart* 2006;**92**:481–486.
20. Alboni P, Brignole M, Menozzi C, Scarfo S. Is sinus bradycardia a factor facilitating overt heart failure? *Eur Heart J* 1999;**20**:252–255.
21. Caliskan K, Balk AHMM, Jordaens L, Szili-Torok T. Bradycardiomyopathy: the case for a causative relationship between severe sinus bradycardia and heart failure. *J Cardiovasc Electrophysiol* 2010;**21**:822–824.
22. Ntalianis A, Nanas JN. Immediate relief of congestive heart failure by ventricular pacing in chronic bradycardia. *Cardiol Rev* 2006;**14**:e14–e15.
23. Alboni P, Scarfo S, Fuca G. Development of heart failure in bradycardic sick sinus syndrome. *Ital Heart J* 2001;**2**:912.
24. Iwataki M, Kim Y-J, Sun B-J, Jang J-Y, Takeuchi M, Fukuda S, Otani K, Yoshitani H, Ohe H, Kohno R, Oginosawa Y, Abe H, Levine RA, Song JK, Otsuji Y. Different characteristics of heart failure due to pump failure and bradyarrhythmia. *J Echocardiogr* 2015;**13**:27–34.
25. Yanni J, D'Souza A, Wang Y, Li N, Hansen BJ, Zakharkin SO, Smith M, Hayward C, Whitson BA, Mohler PJ, Janssen PML, Zeef L, Choudhury M, Zi M, Cai X, Logantha SJRJ, Nakao S, Atkinson A, Petkova M, Doris U, Ariyaratnam J, Cartwright EJ, Griffiths-Jones S, Hart G, Fedorov VV, Oceandy D, Dobrzynski H, Boyett MR. Silencing miR-370-3p rescues funny current and sinus node function in heart failure. *Sci Rep* 2020;**10**:11279.
26. Verkerk AO, Wilders R, Coronel R, Ravesloot JH, Verheijck EE. Ionic remodeling of sinoatrial node cells by heart failure. *Circulation* 2003;**108**:760–766.
27. Csepe TA, Kalyanasundaram A, Hansen BJ, Zhao J, Fedorov VV. Fibrosis: a structural modulator of sinoatrial node physiology and dysfunction. *Front Physiol* 2015;**6**:37–37.
28. Swaminathan PD, Purohit A, Soni S, Voigt N, Singh MV, Glukhov AV, Gao Z, He BJ, Luczak ED, Joiner ML, Kutschke W, Yang J, Donahue JK, Weiss RM, Grumbach IM, Ogawa M, Chen PS, Efimov I, Dobrev D, Mohler PJ, Hund TJ, Anderson ME. Oxidized CaMKII causes cardiac sinus node dysfunction in mice. *J Clin Invest* 2011;**121**:3277–3288.
29. Kalyanasundaram A, Li N, Gardner ML, Artiga EJ, Hansen BJ, Webb A, Freitas MA, Pietrzak M, Whitson BA, Mokadam NA, Janssen PML, Mohler PJ, Fedorov VV. Fibroblast-specific proteotranscriptomes reveal distinct fibrotic signatures of human sinoatrial node in nonfailing and failing hearts. *Circulation* 2021;**144**:126–143.
30. Liu FT, Hsu DK, Zuberi RI, Kuwabara I, Chi EY, Henderson WR Jr. Expression and function of galectin-3, a beta-galactoside-binding lectin, in human monocytes and macrophages. *Am J Pathol* 1995;**147**:1016–1028.
31. Zi M, Stafford N, Prehar S, Baudoin F, Oceandy D, Wang X, Bui T, Shaheen M, Neyses L, Cartwright EJ. Cardiac hypertrophy or failure?—a systematic evaluation of the transverse aortic constriction model in C57BL/6NTac and C57BL/6J substrains. *Curr Res Physiol* 2019;**1**:1–10.
32. Linscheid N, Logantha S, Poulsen PC, Zhang S, Schrölkamp M, Egerod KL, Thompson JJ, Kitmitto A, Galli G, Humphries MJ. Quantitative proteomics and single-nucleus transcriptomics of the sinus node elucidates the foundation of cardiac pacemaking. *Nat Commun* 2019;**10**(1):2889.
33. Lundby A, Andersen MN, Steffensen AB, Horn H, Kelstrup CD, Francavilla C, Jensen LJ, Schmitt N, Thomsen MB, Olsen JV. In vivo phosphoproteomics analysis reveals the cardiac targets of β-adrenergic receptor signaling. *Sci Signal* 2013;**6**(278).
34. Martini E, Kunderfranco P, Peano C, Carullo P, Cremonesi M, Schorn Tilo, Carriero R, Termanini A, Colombo FS, Jachetti E. Single-cell sequencing of mouse heart immune infiltrate in pressure overload–driven heart failure reveals extent of immune activation. *Circulation* 2019;**140**(25):2089–2107.
35. Freshour SL, Kiwala S, Cotto KC, Coffman AC, McMichael JF, Song JJ, Griffith M, Griffith OL, Wagner AH. Integration of the Drug–Gene Interaction Database (DGIdb 4.0) with open crowdsource efforts. *Nucleic Acids Rese* 2021;**49**(D1):D1144–D1151.
36. Ye JZ, Hansen FB, Mills RW, Lundby A. Oncotherapeutic protein kinase inhibitors associated with pro-arrhythmic liability. *JACC: CardioOncol* 2021;**3**(1):88–97.
37. Wiredja DD, Koyutürk M, Chance MR. The KSEA App: a web-based tool for kinase activity inference from quantitative phosphoproteomics. *Bioinformatics* 2017;**33**:3489–3491.
38. Borgo C, D'Amore C, Sarno S, Salvi M, Ruzzene M. Protein kinase CK2: a potential therapeutic target for diverse human diseases. *Signal Transduct Target Ther* 2021;**6**:183.
39. Romero-Becerra R, Santamans AM, Folgueira C, Sabio G. P38 MAPK pathway in the heart: new insights in health and disease. *Int J Mol Sci* 2020;**21**:7412.
40. Wang Y. Mitogen-activated protein kinases in heart development and diseases. *Circulation* 2007;**116**:1413–1423.
41. Szklarczyk D, Gable AL, Nastou KC, Lyon D, Kirsch R, Pyysalo S, Doncheva NT, Legeay M, Fang T, Bork P, Jensen LJ, von Mering C. The STRING database in 2021: customizable protein–protein networks, and functional characterization of user-uploaded gene/measurement sets. *Nucleic Acids Res* 2021;**49**:D605–D612.
42. Hu W, Clark RB, Giles WR, Shibata E, Zhang H. Physiological roles of the rapidly activated delayed rectifier K^+ current in adult mouse heart primary pacemaker activity. *Int J Mol Sci* 2021;**22**:4761.
43. Aslanidi OV, Boyett MR, Dobrzynski H, Li J, Zhang H. Mechanisms of transition from normal to reentrant electrical activity in a model of rabbit atrial tissue: interaction of tissue heterogeneity and anisotropy. *Biophys J* 2009;**96**:798–817.
44. Fenske S, Krause SC, Hassan SI, Becirovic E, Auer F, Bernard R, Kupatt C, Lange P, Ziegler T, Wotjak CT, Zhang H, Hammelmann V, Paparizos C, Biel M, Wahl-Schott CA. Sick sinus syndrome in HCN1-deficient mice. *Circulation* 2013;**128**:2585–2594.
45. Baruscotti M, Bucchi A, Viscomi C, Mandelli G, Consalez G, Gnecchi-Rusconi T, Montano N, Casali KR, Micheloni S, Barbuti A, DiFrancesco D. Deep bradycardia and heart block caused by inducible cardiac-specific knockout of the pacemaker channel gene Hcn4. *Proc Natl Acad Sci U S A* 2011;**108**:1705–1710.
46. Schulze-Bahr E, Neu A, Friederich P, Kaupp UB, Breithardt G, Pongs O, Isbrandt D. Pacemaker channel dysfunction in a patient with sinus node disease. *J Clin Invest* 2003;**111**:1537–1545.
47. Adamo L, Rocha-Resende C, Prabhu SD, Mann DL. Reappraising the role of inflammation in heart failure. *Nat Rev Cardiol* 2020;**17**:269–285.
48. Patel B, Bansal SS, Ismahil MA, Hamid T, Rokosh G, Mack M, Prabhu SD. $CCR2^+$ monocyte-derived infiltrating macrophages are required for adverse cardiac remodeling during pressure overload. *JACC Basic Transl Sci* 2018;**3**:230–244.
49. Fang H, Pengal RA, Cao X, Ganesan LP, Wewers MD, Marsh CB, Tridandapani S. Lipopolysaccharide-induced macrophage inflammatory response is regulated by SHIP. *J Immunol* 2004;**173**:360–366.
50. Monnerat-Cahli G, Alonso H, Gallego M, Alarcón ML, Bassani RA, Casis O, Medei E. Toll-like receptor 4 activation promotes cardiac arrhythmias by decreasing the transient outward potassium current (Ito) through an IRF3-dependent and MyD88-independent pathway. *J Mol Cell Cardiol* 2014;**76**:116–125.

51. Sano H, Hsu DK, Yu L, Apgar JR, Kuwabara I, Yamanaka T, Hirashima M, Liu F-T. Human galectin-3 is a novel chemoattractant for monocytes and macrophages. *J Immunol* 2000; **165**:2156–2164.
52. Felker GM, Fiuzat M, Shaw LK, Clare R, Whellan DJ, Bettari L, Shirolkar SC, Donahue M, Kitzman DW, Zannad F, Piña IL, O'Connor CM. Galectin-3 in ambulatory patients with heart failure: results from the HF-ACTION study. *Circ Heart Fail* 2012;**5**:72–78.
53. Vlachou F, Varela A, Stathopoulou K, Ntatsoulis K, Synolaki E, Pratsinis H, Kletsas D, Sideras P, Davos CH, Capetanaki Y, Psarras S. Galectin-3 interferes with tissue repair and promotes cardiac dysfunction and comorbidities in a genetic heart failure model. *Cell Mol Life Sci* 2022; **79**:250.
54. Frunza O, Russo I, Saxena A, Shinde AV, Humeres C, Hanif W, Rai V, Su Y, Frangogiannis NG. Myocardial galectin-3 expression is associated with remodeling of the pressure-overloaded heart and may delay the hypertrophic response without affecting survival, dysfunction, and cardiac fibrosis. *Am J Pathol* 2016;**186**:1114–1127.
55. Vergaro G, Prud'homme M, Fazal L, Merval R, Passino C, Emdin M, Samuel JL, Cohen Solal A, Delcayre C. Inhibition of galectin-3 pathway prevents isoproterenol-induced left ventricular dysfunction and fibrosis in mice. *Hypertension* 2016;**67**:606–612.
56. Ibarrola J, Sádaba R, Garcia-Peña A, Arrieta V, Martinez-Martinez E, Alvarez V, Fernández-Celis A, Gainza A, Santamaría E, Fernández-Irigoyen J, Cachofeiro V, Fay R, Rossignol P, López-Andrés N. A role for fumarate hydratase in mediating oxidative effects of galectin-3 in human cardiac fibroblasts. *Int J Cardiol* 2018;**258**:217–223.
57. Ibarrola J, Matilla L, Martínez-Martínez E, Gueret A, Fernández-Celis A, Henry J-P, Nicol L, Jaisser F, Mulder P, Ouvrard-Pascaud A, López-Andrés N. Myocardial injury after ischemia/reperfusion is attenuated by pharmacological galectin-3 inhibition. *Sci Rep* 2019;**9**:9607.
58. de Bakker JMT, Wittkampf FHM. The pathophysiologic basis of fractionated and complex electrograms and the impact of recording techniques on their detection and interpretation. *Circ Arrhythm Electrophysiol* 2010;**3**:204–213.
59. Sirish P, Ledford HA, Timofeyev V, Thai PN, Ren L, Kim HJ, Park S, Lee JH, Dai G, Moshref M, Sihn CR, Chen WC, Timofeyeva MV, Jian Z, Shimkunas R, Izu LT, Chiamvimonvat N, Chen-Izu Y, Yamoah EN, Zhang X-D. Action potential shortening and impairment of cardiac function by ablation of Slc26a6. *Circ Arrhythm Electrophysiol* 2017;**10**:e005267.
60. Kodama I, Boyett MR, Nikmaram MR, Yamamoto M, Honjo H, Niwa R. Regional differences in effects of E-4031 within the sinoatrial node. *Am J Physiol* 1999;**276**:H793–H802.
61. Du Y, Zhang J, Xi Y, Wu G, Han K, Huang X, Ma A, Wang T. β1-Adrenergic blocker bisoprolol reverses down-regulated ion channels in sinoatrial node of heart failure rats. *J Physiol Biochem* 2016;**72**:293–302.
62. Mesquita T, Zhang R, Cho JH, Zhang R, Lin YN, Sanchez L, Goldhaber JI, Yu JK, Liang JA, Liu W, Trayanova NA, Cingolani E. Mechanisms of sinoatrial node dysfunction in heart failure with preserved ejection fraction. *Circulation* 2022;**145**:45–60.
63. Estigoy CB, Pontén F, Odeberg J, Herbert B, Guilhaus M, Charleston M, Ho JWK, Cameron D, Dos Remedios CG. Intercalated discs: multiple proteins perform multiple functions in non-failing and failing human hearts. *Biophys Rev* 2009;**1**:43.
64. Kostetskii I, Li J, Xiong Y, Zhou R, Ferrari VA, Patel VV, Molkentin JD, Radice GL. Induced deletion of the N-cadherin gene in the heart leads to dissolution of the intercalated disc structure. *Circ Res* 2005;**96**:346–354.
65. Li J, Patel VV, Kostetskii I, Xiong Y, Chu AF, Jacobson JT, Yu C, Morley GE, Molkentin JD, Radice GL. Cardiac-specific loss of N-cadherin leads to alteration in connexins with conduction slowing and arrhythmogenesis. *Circ Res* 2005;**97**:474–481.
66. Mezzano V, Liang Y, Wright AT, Lyon RC, Pfeiffer E, Song MY, Gu Y, Dalton ND, Scheinman M, Peterson KL, Evans SM, Fowler S, Cerrone M, McCulloch AD, Sheikh F. Desmosomal junctions are necessary for adult sinus node function. *Cardiovasc Res* 2016;**111**:274–286.
67. Olshansky B, Sabbah HN, Hauptman PJ, Colucci WS. Parasympathetic nervous system and heart failure: pathophysiology and potential implications for therapy. *Circulation* 2008;**118**:863–871.
68. Strassheim D, Dempsey EC, Gerasimovskaya E, Stenmark K, Karoor V. Role of inflammatory cell subtypes in heart failure. *J Immunol Res* 2019;**2019**:2164017.
69. Murphy Sean P, Kakkar R, McCarthy Cian P, Januzzi James L. Inflammation in heart failure. *J Am Coll Cardiol* 2020;**75**:1324–1340.
70. Suthahar N, Meijers WC, Silljé HHW, de Boer RA. From inflammation to fibrosis-molecular and cellular mechanisms of myocardial tissue remodelling and perspectives on differential treatment opportunities. *Curr Heart Fail Rep* 2017;**14**:235–250.
71. Moskalik A, Niderla-Bielińska J, Ratajska A. Multiple roles of cardiac macrophages in heart homeostasis and failure. *Heart Fail Rev* 2022;**27**:1413–1430.
72. Lavine KJ, Epelman S, Uchida K, Weber KJ, Nichols CG, Schilling JD, Ornitz DM, Randolph GJ, Mann DL. Distinct macrophage lineages contribute to disparate patterns of cardiac recovery and remodeling in the neonatal and adult heart. *Proc Natl Acad Sci U S A* 2014;**111**: 16029–16034.
73. Sager HB, Hulsmans M, Lavine KJ, Moreira MB, Heidt T, Courties G, Sun Y, Iwamoto Y, Tricot B, Khan OF, Dahlman JE, Borodovsky A, Fitzgerald K, Anderson DG, Weissleder R, Libby P, Swirski FK, Nahrendorf M. Proliferation and recruitment contribute to myocardial macrophage expansion in chronic heart failure. *Circ Res* 2016;**119**:853–864.
74. Lazzerini PE, Capecchi PL, El-Sherif N, Laghi-Pasini F, Boutjdir M. Emerging arrhythmic risk of autoimmune and inflammatory cardiac channelopathies. *J Am Heart Assoc* 2018;**7**:e010595.
75. Sharma UC, Pokharel S, van Brakel TJ, van Berlo JH, Cleutjens JPM, Schroen B, André S, Crijns HJGM, Gabius H-J, Maessen J, Pinto YM. Galectin-3 marks activated macrophages in failure-prone hypertrophied hearts and contributes to cardiac dysfunction. *Circulation* 2004;**110**:3121–3128.
76. Liu Y-H, D'Ambrosio M, Liao TD, Peng H, Rhaleb N-E, Sharma U, André S, Gabius H-J, Carretero OA. N-acetyl-seryl-aspartyl-lysyl-proline prevents cardiac remodeling and dysfunction induced by galectin-3, a mammalian adhesion/growth-regulatory lectin. *Am J Physiol Heart Circ Physiol* 2009;**296**:H404–H412.
77. Martínez-Martínez E, Calvier L, Fernández-Celis A, Rousseau E, Jurado-López R, Rossoni LV, Jaisser F, Zannad F, Rossignol P, Cachofeiro V, López-Andrés N. Galectin-3 blockade inhibits cardiac inflammation and fibrosis in experimental hyperaldosteronism and hypertension. *Hypertension* 2015;**66**:767–775.
78. Yu L, Ruifrok WP, Meissner M, Bos EM, van Goor H, Sanjabi B, van der Harst P, Pitt B, Goldstein IJ, Koerts JA, van Veldhuisen DJ, Bank RA, van Gilst WH, Silljé HH, de Boer RA. Genetic and pharmacological inhibition of galectin-3 prevents cardiac remodeling by interfering with myocardial fibrogenesis. *Circ Heart Fail* 2013;**6**:107–117.
79. Wu C, Lv Z, Li X, Zhou X, Mao W, Zhu M. Galectin-3 in predicting mortality of heart failure: a systematic review and meta-analysis. *Heart Surg Forum* 2021;**24**:E327–E332.
80. de Boer RA, Voors AA, Muntendam P, van Gilst WH, van Veldhuisen DJ. Galectin-3: a novel mediator of heart failure development and progression. *Eur J Heart Fail* 2009;**11**:811–817.
81. Boyett MR, Honjo H, Kodama I. The sinoatrial node, a heterogeneous pacemaker structure. *Cardiovasc Res* 2000;**47**:658–687.
82. Tellez JO, Dobrzynski H, Greener ID, Graham GM, Laing E, Honjo H, Hubbard SJ, Boyett MR, Billeter R. Differential expression of ion channel transcripts in atrial muscle and sinoatrial node in rabbit. *Circ Res* 2006;**99**:1384–1393.
83. Arrieta V, Martinez-Martinez E, Ibarrola J, Alvarez V, Sádaba R, Garcia-Peña A, Fernández-Celis A, Cachofeiro V, Rossignol P, López-Andrés N. A role for galectin-3 in the development of early molecular alterations in short-term aortic stenosis. *Clin Sci (Lond)* 2017;**131**:935–949.
84. Martínez-Martínez E, López-Ándres N, Jurado-López R, Rousseau E, Bartolomé MV, Fernández-Celis A, Rossignol P, Islas F, Antequera A, Prieto S, Luaces M, Cachofeiro V. Galectin-3 participates in cardiovascular remodeling associated with obesity. *Hypertension* 2015;**66**:961–969.
85. Takemoto Y, Ramirez RJ, Yokokawa M, Kaur K, Ponce-Balbuena D, Sinno MC, Willis BC, Ghanbari H, Ennis SR, Guerrero-Serna G, Henzi BC, Latchamsetty R, Ramos-Mondragon R, Musa H, Martins RP, Pandit SV, Noujaim SF, Crawford T, Jongnarangsin K, Pelosi F, Bogun F, Chugh A, Berenfeld O, Morady F, Oral H, Jalife J. Galectin-3 regulates atrial fibrillation remodeling and predicts catheter ablation outcomes. *JACC Basic Transl Sci* 2016;**1**: 143–154.
86. Vizcaíno JA, Csordas A, del-Toro N, Dianes JA, Griss J, Lavidas I, Mayer G, Perez-Riverol Y, Reisinger F, Ternent T, Xu QW, Wang R, Hermjakob H. 2016 update of the PRIDE database and its related tools. *Nucleic Acids Res* 2016;**44**:D447–D456.